Alexandre Ernesto Grüninger de Oliveira

Licenciatura em Engenharia de Materiais

Cellulose micro/nano fibers conformational effects probed by nematic liquid crystal droplets

Dissertação para obtenção do Grau de Mestre em
Engenharia de Micro e Nanotecnologias

Orientador: Professora Doutora Maria Helena Godinho, Professora Auxiliar com Agregação, Departamento Ciência dos Materiais, Faculdade de Ciências e Tecnologia da Universidade Nova de Lisboa

Co-orientador: Doutor Luis Ever Aguirre, Pós-Doc CENIMAT/I3N e Departamento de Ciências dos Materiais, Faculdade de Ciências e Tecnologia da Universidade Nova de Lisboa

Júri:

Presidente:	Prof. Doutor Rodrigo Martins
Arguente:	Prof. Doutor Pawel Pieranski
Vogal:	Doutor Luis Aguirre

FACULDADE DE CIÊNCIAS E TECNOLOGIA
UNIVERSIDADE NOVA DE LISBOA

Setembro 2014

Cellulose micro/nano fibers conformational effects probed by nematic liquid crystal droplets

Acknowledgments

Agradeço à professora Helena Godinho por todo o apoio durante a realização desta dissertação. Não agradeço apenas pela ajuda, mas pela forma como conduziu todo o projeto, pela sua total dedicação e empenho, pela sua tão característica e evidente paixão e motivação colocadas em todas as etapas.

Al Doctor Luís Aguirre, que más que como mi co-orientador, lo considero como un ejemplo de integridad, de profesionalidad y dedicación. Además de una ayuda constante, él me ha enseñado verdaderamente a investigar y a ser crítico con los resultados. Estoy muy grato por su forma muy particular de animarme y por su apoyo que no me dejo desfallecer para así poder llevar a cabo la culminación de este proyecto. Me ha llevado tiempo, pero ahora sí comprendo que el sol también brilla aunque el cielo esté nublado. Sin embargo, sigo sin entender cómo es posible que alguien diga que las hamburguesas con chimichurri son mejores que el serra da estrela?!

In addition, a special thank you to Prof. Slobodan Zumer and Doctor David Sec from the University of Ljubljana, Slovenia, for their collaboration and help during this project.

I would also like to express my deepest appreciation to the committee member, Professor Pawel Pieranski, who graciously accepted to be part of the jury, which is for me a tremendous honor.

Ao Prof. Rodrigo Martins e Prof. Elvira Fortunato pelo desenvolvimento e reconhecimento que alcançaram para o curso de Engenharia de Materiais e pela criação e promoção do curso de Engenharia Micro e Nanotecnologias.

Ao longo destes anos tantas as pessoas que me passaram na minha vida e tão pouco o espaço e tempo para as agradecer. Gostaria, porém de deixar uma pequena frase agradecimento àquelas que mais que um apoio, me ensinaram algo:

À Joana Fernandes por estes cinco anos e por me fazeres acreditar que nenhum programa de edição de Figurem por mais avançado conseguirá alguma vez ultrapassar a perfeita combinação Paint - Power Point.

Migsy Pontes, para que saibas, enquanto escrevia os agradecimentos deparei-me com um concurso para uma star-up… e outro de empreendedorismo? Espera, talvez prefiras o de inovação? Podemos fazer os três, empreendedorismo, inovação e novas ideias de negócio!? Juntos desabrochámos esta veia empreendedora e descobrimos esta vocação neste mundo que tanto necessita deste nosso espirito empreendedor. (consegui?)

À Teresa Kullberg, a rainha das pastilhas elásticas, agradeço por me fazer ver que o viscosímetro é algo divertido, fantástico, dinâmico e inovador.

Migsy Princesa Trofas pela amizade, pelo café Timor, pelo chá (se bem que não se convida um amigo para tomar chá) e pelos diversos e mais variados salmões. Prometo que um dia vamos conseguir ver o Sansouci, à terceira é de vez!

Ao Ricardo Marreiros por me mostrar que é possível sair à rua, orgulhosamente, combinando azul, vermelho, amarelo, verde, preto e laranja (penso que não falta nenhuma).

Ao Zé Rui pela inócua fartura que nunca vi e à Susana em virtude da tua ajuda, obrigado.

Um agradecimento à Doutora Coro Echeverria e à Mestre Paula Soares por me tentarem mostrar que existe uma vida para além da tese…ainda a procura, mas penso que se escondeu. Um dia poderemos debater este tema no lugar da gente jovem…

Ich möchte mich bei meiner Mutter und meinen Geschwistern und Professor Doktor Jaap Hoepelmann möchte ich mich ganz besonders herzlich bedanken für die uneingeschränkte, liebevolle und vielseitige Unterstützung während meines Studiums, ohne die diese Arbeit so nicht möglich gewesen wäre.

Abstract

Probing micro-/nano-sized surface conformations, which are ubiquitous in biological systems, by using liquid crystal droplets, which change their ordering and optical appearance in response to the presence of more than ten times smaller cellulose based micro/nano fibers, might find new uses in a range of biological environments and sensors. Previous studies indicate that electrospun micro/nano cellulosic fibers produced from liquid crystalline solutions could present a twisted form [1]. In this work, we study the structures of nematic liquid crystal droplets threaded by cellulose fibers prepared from liquid crystalline and isotropic solutions as well as droplets pierced by spider-made fibers [2]. Planar anchoring at the fibers and planar and homeotropic at the drop surfaces allowed probing cellulose fibers different helical structures as well as aligned filaments.

Keywords: Droplets, cellulose, micro/nano fibers, anchoring, conformation

Resumo

A existência de conformações na superfície dos materiais à micro/nano escala são ubíquas em sistemas biológicos e complexos. Neste contexto, esta tese pretende desenvolver um método simples de visualização e quantificação deste tipo de conformações por meio da utilização de gotas de cristal liquido e da sua intrínseca capacidade de alterar a organização molecular e consequente alteração da sua aparência ótica aquando da presença micro/nano imperfeições periódicas suaves ou modulações presentes nas fibra.

Estudos anteriores evidenciam que micro/nano fibras de celulose produzidas através da técnica de electrofiação a partir de soluções na fase liquidas-cristalina podem apresentar uma forma helicoidal. Neste trabalho, são estudadas as estruturas das gotas de cristal liquido nemático quando perfuradas por fibras de celulose preparadas por soluções tanto na fase liquida cristalina, como na fase isotrópica, assim como gotas perfuradas por sistemas altamente complexos, como o caso das teias de aranha.

A ancoragem planar induzida junto à fibra e ancoragem planar ou homeotrópica promovida na superfície da gota permite a deteção de variações morfológicas na superfície da fibra devido a alterações detetáveis nas estruturas da gota, nomeadamente quantificação da quiralidade induzida pela fibra.

Palavras-chave: Gotas, celulose, micro/nano fibras, ancoragem, conformação

Abbreviations

3D	Three dimensional
5CB	4'-n-pentyl-4-cyanobiphenyl
CA	Cellulose acetate
DMac	Dimethylacetamide
DS	Average of degree of substitution
HPC	Hydroxypropylcellulose
LC(s)	Liquid crystal(s)
NI	Nematic to isotropic
POM	Polarizing optical microscopy
SEM	Scanning electronic microscopy

Symbols

A	Area of the bounding surface
F	Free energy
F_s	Free energy from the surface confinement
F_v	Free energy from the bulk
K	Frank elastic constant
K_{11}	Splay elastic constant
K_{22}	Twist elastic constant
K_{24}	Saddle-splay elastic constant
K_{33}	Bend elastic constant
Q	Topological charge
R	Droplet radius
s	Defect strength
S	Order parameter
σ	Surface free energy per unit area
T	Temperature
t	Time
v	Volume
W	Anchoring energy
wt%	Weight percentage
λ	Wavelength

Table of Contents

Acknowledgments ..... **v**

Abstract ..... **vii**

Resumo ..... **ix**

Abbreviations ..... **xi**

List of Figures ..... **XVII**

Objective **1**

Chapter 1 – Introduction **3**

1.1. Motivation **3**

1.2. Overview on liquid crystals **3**

1.3. Nematic Phase **4**

1.3.1. Order Parameter 5

1.3.1.1. Deformation mechanisms 6

1.3.1.2. Disclinations 6

1.4. Liquid crystal drops and shells **7**

1.5. Fibers and process **9**

Chapter 2 – Experimental and Characterization Techniques **11**

Chapter 3 – Results and Discussion **13**

3.1 Fiber characterization **13**

3.3 Liquid crystal droplets pierced by spider silk fibers **22**

Chapter 4 – Conclusions and Future Perspectives **29**

Bibliography **31**

Appendix **35**

List of Figures

Figure 1.1- Coordinates of the rod used to define the order parameter tensor. 5
Figure 1.2 – Basic types of deformation occurring in nematics for strong surface anchoring conditions. a)Twist, K_{22}; b) Splay, K_{11}; c) Bend, K_{33} 6
Figure 1.3 - Schematic of the nematic drops with different structures a) radial drop, with one radial hedgehog at the center of the sphere, regularly observed when the anchoring is perpendicular; b) bipolar drop, with two s=1 splay-type boojums located on the surface, regularly observed for planar anchoring conditions. 9
Figure 1.4 - Schematic representation of the electrospinning setup. 10
Figure 2.1 – Schematics of the experimental Setup. The electrospinning target used to produce the air suspended fibers with numerous 5CB liquid crystal droplets b) cross-polarized Figure corresponds to nematic droplets constrained on a thin fiber (2,0 micrometers) c) Cross-polarized, with retardation plate and bright field Figures of 5CB droplets involved in optimized glycerol solution, planar anchoring. 12
Figure 3.1 - SEM Figures of electrospun fibers a) cellulose acetate fibers produced from an isotropic solution (12%w/w) b) Hydroxypropylcellulose fiber prepared from a solution in the liquid crystalline phase (60% w/w). 13
Figure 3.2 – Schematic of the director field configuration (a) air floating nematic shell constrained in a fiber, thus adding an additional cylindrical surface with planar anchoring along the droplets long axis and perpendicular at the outer surface (b) Bright field Figure example of a nematic drop threaded by cellulose acetate fiber. The Figure appears defocused to highlight the ring disclination. The scale bar corresponds to 10 µm. 14
Figure 3.3 – SEM Figures of electrospun fibers and POM pictures of nematic bead textures. i) from cellulose acetate fibers produced from an isotropic solution (12%w/w) ii) hydroxypropylcellulose fiber prepared from a solution in the liquid crystalline phase (60% w/w). a) SEM Figures (b-d) POM pictures of 5 CB liquid crystal droplets threaded by a thin cellulosic-made fibers with planar anchoring at the fiber and homeotropic anchoring at the air interface b) under parallel polarizers c) under cross-polarizers picture d) with a 530nm full retardation plate, between cross-polarizers. 15
Figure 3.4 – Heating of a ring structure nematic droplet suspended in air. The heating rates are both equal to 1ºC/min. Heating snapshot Figures represent the time evolution of the nematic droplet from the equilibrium director configuration (t=0s) to the quasi-isotropic phase. a)droplet pieced by hydroxypropylcellulose fiber b) droplet pierced by cellulose acetate fiber. The scale bar corresponds to 10 µm. 18
Figure 3.5 – Cooling processes of a ring structure nematic droplet suspended in air. The cooling rates are both equal to 1ºC/min. Cooling snapshot Figures represent the time evolution of the nematic droplet from the quasi-isotopic phase (t=0s) to the ring configuration. a) droplet pierced by hydroxypropylcellulose fiber b) droplet pierced by cellulose acetate fiber. The scale bar corresponds to 10 µm. 20

Figure 3.6 – POM Figures of 5CB droplets surrounded by a shell of glycerol which encloses the liquid crystal and suspended in air by a thin cellulosic-made fiber. (a-b) Hydroxypropil cellulose fiber prepared from liquid crystalline phase a) presenting a right-handed twist b) presenting a left-handed twist c) Cellulose acetate fiber prepared from the isotropic solution, presenting no-handed twist. The scale bar corresponds to 10 µm. 21
Figure 3.7 - Numerically calculated structures in nematic drops threaded on thin cellulosic fibers with planar – planar configuration a) right-handed fiber b) non-handed fiber c) left handed fiber. Note the resemblance of the micrographs with experiments, namely the ring location. 22
Figure 3.8 - POM pictures of nematic bead textures pierced by spider-made fibers. a) from an inner-spider b) from a garden spider. The scale bar corresponds to 10 µm. 22
Figure 3.9 - SEM Figures of inner-spider web used to thread the 5CB liquid crystal with different magnifications in order to highlight the fiber´s surface. 23
Figure 3.10 - Numerically calculated structures in nematic drops threaded on a spider web fiber suspended in air a) with infinite tangential orientation of the molecules at the fiber b) tangential at 45º c) with a slightly chirality. 24
Figure 3.11 – Melting process of ring defects and ring defect generation process of a 5CB liquid crystal threaded by an inner spider web fiber with infinite tangential alignment at the fiber´s surface and suspended in air. a) Heating snapshot Figures represent the time evolution of the nematic droplet from the equilibrium director configuration (t=0s) to the quasi-isotropic phase (t=34s) at a constant heating rate of 0,1ºC/min. b) Cooling snapshot Figures represent the time evolution of the nematic droplet from the isotopic phase (t=0s) to the stable anisotropic configuration (t=93s) at a constant cooling rate of 1ºC/min. ..... .28
Figure 3.12 - Melting process of ring defects and ring defect generation process of a 5CB liquid crystal threaded by a garden spider web fiber with slightly chiral alignment at the fiber´s surface and suspended in air. a) Heating snapshot Figures represent the time evolution of the nematic droplet from the equilibrium director configuration (t=0s) to the quasi-isotropic phase (t=71,3s) at a constant heating rate of 0,1ºC/min. b) Cooling snapshot Figures represent the time evolution of the nematic droplet from the isotopic phase (t=0s) to the stable anisotropic configuration (t=81,3s) at a constant cooling rate of 1ºC/min. 27

Objective

With the advent of nanotechnology liquid-crystalline materials are nowadays studied with regard to their interaction with specific surface structures. The framework of this thesis aims to investigate the influence of exoteric configurations of the director field, by changing the anchoring conditions as well as the temperature role in the evolution of defects observed in liquid crystals droplets pierced by micro/nano fibers.

.

Chapter 1 – Introduction

1.1. Motivation

Today´s systems mainly depend on the top-down approach, hence they are composed by multiple components, thus having various interfaces and complex interactions. Understanding the synergy of these factors and their impact on material properties presents a great scientific challenge as it is expected that in the near future low-cost, miniaturized, tunable and high performance devices will be developed.

However, if we look at the matter in an unconventional and innovative way, the bottom up approach involving self-assembling components constitutes a better and easier way to produce cheap, complex shapes and nano-sized devices with self-healing properties[1,2].

Advances in this respect hold the promise of creating novel materials, exploiting these same distinctive features for new materials design with new levels of functionality similar to those existing in nature [3].

Consequently, hybridization of soft matter science involving a broad spectrum of different scientific disciplines, namely physics, chemistry and biology, is highly appealing mainly due to the astounding properties of soft matter materials as mentioned above.

Recent research, namely the work carried out by Geng *et al*.[4] in which cholesteric microdroplets are pierced by a cellulose fiber, shows a broad new range of opportunities, as breaking up the spherical symmetry of the liquid crystal droplets gives rise to exotic topological defects showing interesting possibilities for coupling optical fibers to liquid crystal microresonators[4] taking the outstanding work reported by Musevic *et al*. where the first tunable and omnidirectional soft-mater 3D lasers were realized[5]. A similar breakthrough was made when Fukuda et al.[6] reported a liquid-crystal-based chirality balance offering a quick and versatile chirality-sensing method for gas-phase analysis. Their preliminary results may play a vital role in the pharmaceutical industry, on-site drug analysis or other environmental chemicals as well as to the fragrance and perfume industry.

With the advent of nanotechnology, this project exploits liquid crystalline materials not only their sensing properties, where helical conformations can be probed, but at the same time their interaction with specific surface structures and the influence of combined external stimuli: anchoring conditions and temperatures that could reinforce the properties stimulating the appearance of sophisticated structures supporting the development of new fields such as the nanophotonics, or polymeric fiber technology, nanoconfinement or in more futuristic view: development of topological memory devices and novel types of self-assembly[7-11].

1.2. Overview on liquid crystals

By the end of the nineteenth century, science made a new breakthrough with an idea that challenged the scientific community: the discovery of the fourth state of matter - liquid crystals[12].

It was known that ordinary liquids and gases did not present any long range order and thus were considered as amorphous phases whereas solids could be either crystalline and/or amorphous. By definition and regarding solely the crystalline domains, all the components (such as molecules or atoms) are regularly stacked, having their centers of gravity periodically located into a 3D lattice[13-15].

Interestingly enough, many existing phases in nature present a more ordered structure than isotropic liquids, yet less ordered than typical crystals. These peculiar phases are grouped together and are coined liquid crystals or mesomorphic materials, since they share properties normally associated with both the liquids and crystals [16,17].

Roughly speaking, mesomorphic materials can be seen as ordered liquids or alternatively as disordered solids, as one is confronted with a system displaying spatial liquid-like order and at the same time some degree of anisotropy: anisotropic fluids [18].

Therefore mesogenic substances (molecule or group of molecules responsible for generating mesophases) can be classified according to their shape, where rod-like (calamitic), and disk-like molecules (discotic) are the most ordinary ones. In this category, substances may present one or more phases (polymorphism) as they are heated up or cooled down – thermotropic liquid crystals. Yet, if the mesomorphic character appears in a solution with an appropriate solvent under a certain and well defined range of concentration, pressure and temperature, the liquid crystal is called lyothropic.

Regarding the structure of the mesophase, three main classes arise: nematics, smectics and columnar, differing from their molecular arrangement and in turn different macroscopic symmetries and physical properties[12,13].

1.3. Nematic Phase

Etymologically, the word nematic, from Greek "νῆμα" - thread, refers to the thread-like defects in its anisotropy which can regularly be seen when observing this particular phase under polarized light. These so called threads have scientifically been termed "disclinations lines" by Frank in analogy to dislocations in certain defects in solids (highlighted in 1.3.1.2) [19].

The essential difference in these systems, as mentioned before, is the molecular anisotropy which is obviously a precondition for macroscopic anisotropy. An increase in either the shape anisotropy (steric effect), or in the anisotropy polarisabilty (thermotropic effect) leads to anisotropic liquids with long range directional ordering. Generally speaking it can be explained by the molecule´s shape that stimulates other molecules to align themselves in parallel as they can turn more freely without overlapping [18].

The other ordering mechanism - thermotropic effect - helps explain the phenomenon observed in figures 3.5, 3.6, 3.11 and 3.12 where a reduction in temperature leads to nematic ordering (phenomena which will be further highlighted in chapter 3).

If we consider pairs of molecules it is known that a fluctuation of electron density gives rise to a dipole moment and so to an electric field at the neighboring molecule, that will consequently and spontaneously induce a second and opposite (in direction) dipole. Both will definitely attract each other, seeking the lowest energy configuration. One would expect that the molecular configuration that allows a higher aspect to the electric field created, will consequently induce a greater dipole and thus create a greater attraction between both molecules which will than lower the energy of the pair of molecules.

It is than explained, by the hybridization of both effects (steric and thermothropic effect), the strong correlation between the orientation of a random molecule and the orientation of its neighboring molecules in the nematic phase. As seen before, this long-range uniaxial orientational order is encouraged by short-distance interactions, ultimately every molecule will have its orientation parallel to the orientation of the neighboring molecules throughout the sample [13].

On the other hand, the gravity centers of the constituent molecules in the nematic phase do not present any long-range correlation, similarly to conventional liquids.

This preferential molecular alignment is mathematically represented as a unit vector, $\vec{n}$, since its magnitude has no physical significance, labeled director. Furthermore, the capability to rotate around the long axes and the lack of preference concerning the ends of the molecule due to the non-polar nature of this phase, leads to $\vec{n} = -\vec{n}$ [20].

1.3.1. Order Parameter

We have seen before that liquid crystals present a liquid-like order at least in one direction, being more ordered (thus having less symmetry) than liquids due to the inherent tendency of their constituent molecules to align parallel to some common axis[14].

This particular characteristic makes liquid crystals, and more specifically, nematics, optically uniaxial materials with very large birefringence and anisotropic properties that can be further exploited for both scientific and practical interests [2].

However, due to thermal fluctuations, this alignment may suffer some deviations around a statistical value. As a result one should be able to quantitatively express this average orientation: as an order parameter [15].

By assuming a perfect cylindrical symmetry of the rigid rod-like molecule about the unit vector, $\vec{n}$, it is possible to define the director´s coordinates, Figure 1.1:

$$\vec{n}_x = sin(\theta) \cdot cos(\varphi)$$
$$\vec{n}_y = sin(\theta) \cdot sin(\varphi)$$
$$\vec{n}_z = cos(\theta)$$

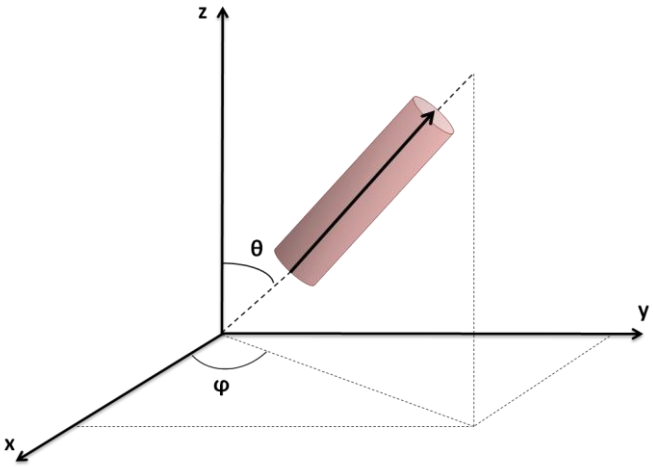

Figure 1.1- Coordinates of the rod used to define the order parameter tensor.

The molecular alignment state can be described by the distribution function f(θ,ϕ)dθ, where f(θ,ϕ) is the probability of finding an arbitrary main axis of a certain molecule, $\vec{n}$, within a small angle dθ around the direction (θ,ϕ). Once the rod possesses a complete cylindrical symmetry around the director, f(θ,ϕ) is independent of ϕ, thus $\vec{n} = -\vec{n}$ as already been mentioned.

$$d\Omega = sin(\theta)\, d\theta d\varphi$$
$$\theta = [0; \pi]$$
$$\varphi = [0; 2\pi]$$

The order parameter is given by:[13]

$$S = \frac{1}{2}\langle 3\, cos^2(\theta) - 1 \rangle \qquad \text{(equation 1)}$$

The order parameter decreases with increasing temperature: for temperatures higher than the nematic-isotropic transition, the order parameter equals zero, which is a direct consequence of the complete random orientation, the main attribute of the isotropic phase.

Accordingly, for an ideal crystal: *S*=1; while for an isotropic phase: *S*=0, whereas in the nematic phase is located between 0 and 1 [13,21].

1.3.1.1. Deformation mechanisms

Theoretically, when undeformed, nematic uniaxial liquid crystal´s director points, on average, in the same linear direction - $\pm\vec{n}$ - throughout the sample. Yet, owing to their intrinsic high fluidity, such systems are highly susceptible to deformation whenever restricted by any limiting conditions, leading to a variation in the director´s direction from point to point.

In relation to the previous example, it is also important to take into account the constrains imposed by the limiting surfaces or external forces acting upon the liquid crystal system. Therefore it is important to quantitatively define the equilibrium state of a nematic liquid crystal achieved when the director shows no spatial variation. Otherwise, there will be an increase of the free energy density of the system, as it costs energy to induce any kind of curvature in the director field, thus increasing the instability of the system.

In other words and according to Frank´s continuous elastic theory, it is possible to quantitatively evaluate the energetic cost to overcome the elastic distortion. This energy is given by the sum of the three basic types of deformations: splay, twist and bend[13,21].

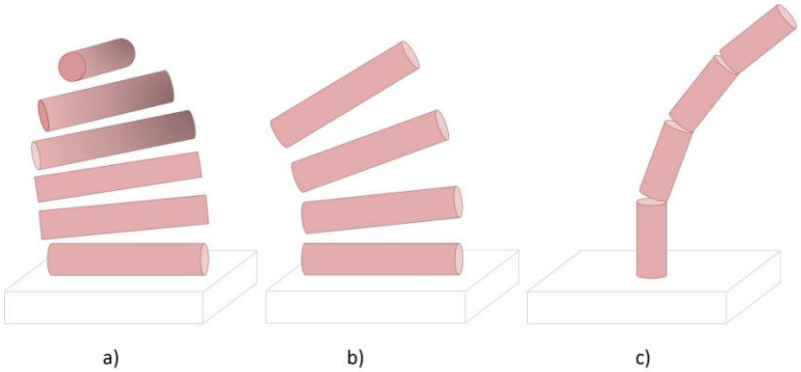

Figure 1.2 – Basic types of deformation occurring in nematics for strong surface anchoring conditions. a)Twist, K_{22}; b) Splay, K_{11}; c) Bend, K_{33}

$$F_d = \frac{1}{2}\cdot K_{11}(div\ n)^2 + \frac{1}{2}K_{22}(n\cdot \Delta n)^2 + \frac{1}{2}K_{33}[n\times(\Delta\cdot n)]^2 - K_{24}div[n\ div\ n + n\ \times(\Delta\cdot n)]$$

(equation 2)

Although the saddle-splay contribution - K_{24} - term does not change the bulk equilibrium equations, thus being normally ignored, it has to be taken into account whenever topological changes occur, such as transformation of the spherical-like core of the hedgehog into a torus-like core of the disclination ring with a macroscopic radius much larger than the nematic coherence length[22].

All K_{ii} constants must always be positive, insuring the thermodynamical stability of the system as they represent Frank´s elastic constants associated with the ability of the director to resist splay, K_{11}, twist, $K_{22,}$ and bend, K_{33}[21,23].

1.3.1.2. Disclinations

So far variations in the director orientation have been considered to be smooth, enabling a fine definition of the director field. Considering the same liquid-crystal system, and assuming it is confined in a container, the director´s orientation will suffer an abrupt alteration in relation to the neighboring directors due to the molecule-container anchoring.

This phenomenon is known as “anchoring” and can happen whenever there are changes in the boundary conditions or an external field is applied, giving rise to three different possible types of defects: point disclinations, lines and walls[13,23,26].

However there is an energetic cost to deviate the director from the easy axis, which is quantitevely defined by the anchoring energy of adjacent surface area. Therefore, the closer the director to the surface the stronger the influence of the surface upon this last one. The alignment effects of the boundaries are also transmitted to the bulk region. Hence the director´s orientation in the bulk is different from the one found near the surface.

The important parameter characterizing the surface anchoring strength is the penetration-length given by L~K/W, where *K* is an elastic constant and *W* the anchoring energy. The penetration-length means the distance from the real surface where the director would coincide with the easy axis orientation. If the anchoring energy is infinitely large, than the penetration length is approximately zero and the director coincides with easy axis orientation near the surface.

Upon these deviations in the director field, topological defects will arise (as a direct consequence of breaking the continuous symmetry). In this way, orientational order can be locally disrupted (so that the director field cannot be defined any longer) leading to defects named “disclinations” [24,25].

Thermodynamically speaking, a given system always evolves towards the equilibrium - lowest state of energy – and so does the chain of defects. As a matter of fact, defects like point disclinations, located at the boundary surface, tend to extinguish one another and line disclinations, normal to the surface´s plane, tend to stretch to minimize the energy[13,27].

In this respect the modulation of the director is highly interesting, since it directly affects the stability of complex phases or the modulation of physical phenomena, i.e. phase transitions.

The overall alignment is therefore very sensitive to the external fields, the strength and type of local molecular anchoring at the interface[2,28-30].

1.4. Liquid crystal drops and shells

The renowned properties of liquid crystals and their micro-/nano-scale exotic behavior are currently of great interest in a broad range of research areas such as optical light-trapping [31], optofluidics[32], sensors[6], photonics[2,33,34] and colloidal science[35].

Regarding this project, one will center on the article reported by Musevic et al. on 3D microlasers self-assembled cholesteric liquid crystal microdroplets, work that may herald a new era of photonics and will undoubtedly help developing other fields such as telecommunications and holographic displays[36].

In this context, a work carried out by Godinho *et al*.[4] introduced a all new perspective to these cholesteric microlasers when the perfect spherical geometry of the cholesteric liquid-crystal microdroplets was disrupted by piercing a thin long fiber. Furthermore Geng *et al*.[37] were able to visualize the electrical response of a nematic liquid crystal drop of toroidal topology threaded in cellulosic fibers, suspended in air, which surprisingly lead to the appearance of a solution–like particle orbiting around the fiber at the center of the liquid crystal drop. Moreover it was possible to investigate non-trivial point defects - energetically unstable - by forcing the system to undergo a phase transition.

The study regarding liquid crystal droplets and their intrinsic topology is fascinating not only regarding the understanding of fundamental physics, but for many practical applications, as a controlled orientation of the molecules in a particular direction is highly desired, which can either be achieved by confining a thin layer of liquid crystal by some external surfaces or by encapsulating the liquid crystal inside a carrying material, leading to liquid crystal droplets formation[38].

Strictly speaking, one can define a liquid crystal droplet as a spherical or ellipsoidal volume generally dispersed in a polymer matrix or in another liquid. Whether suspended or in solution, a liquid crystal droplet is characterized by the ordered inner structure of the dispersed particles and its small scale confinement (in the micrometers range) in which a number of forces, namely bulk and surface interactions, are in direct competition[39].

Independently of the nature of the droplet (liquid crystal, isotropic droplets or monodomain solid crystals) once bounded by an isotropic medium, the free energy is given by sum of the free energy from the bulk and from the surface confinement [40]:

$$F = F_V + F_S = \int_V f dV + \int_S \sigma dS \qquad \text{(equation 3)}$$

This subtle interplay among bulk and surface energies reaches its equilibrium state when the total free energy is minimized. The problem regarding this energy minimization arises since σ depends on the surface orientation of the liquid crystal molecules, leading to practically spherical shape droplets as the energy required to extend the area of the surface while preserving the equilibrium state of the director is much higher than the anchoring energy.

Moreover both the surface and bulk energies in these materials are comparable. As a result the structure is greatly influenced by the droplet´s size. In small droplets the director tends to be uniform as the surface energy cannot outweigh the bulk energy for radius typically R<K/W[23,40].

Energetically speaking, curved boundary conditions are very costly thus an increase in the droplets size leads to an increase in the elastic free energy so that in large droplets, molecules will be aligned along the easy direction, which will than distort the director in the bulk, while at the same time the bulk contribution plays a smaller role.

Whenever the orientation field surrounding the droplet comes into conflict with the far-field orientation of the molecules, elastic energy density grows sufficiently large, so that the order parameter cannot be transformed into a uniform state[40]. These highly energetic structures force the nematic system to adopt a configuration which minimizes both the number and strength of those defects in order to reach an equilibrium state. For that reason singularities can be formed during symmetry-breaking, phase transitions or under the influence of external fields, i.e. by changing the anchoring conditions so that one can easily convince oneself that topological defects are necessary elements of an equilibrium state[24,41].

Nevertheless their stability can only be guaranteed by the conservation of its topological charge (total sum of the disclinations charges vanishes throughout the sample)[42]. This same simple principle regulates the decay and merging of effects, their creation, annihilation or transformation.

As a result of confining a nematic liquid crystal to a spherical volume, topological constraints on the director field are inevitable, leading to the presence of defects which are characterized by their topological charge *s*, quantifying how much the director is rotated about the defect core.

Nonetheless the possible director configurations within this geometry is restricted due to Poincaré-Hopf theorem for tangential or parallel of the director to the bounding surface to those containing total topological charge of *s*=+2 on the drop surface. Conversely, when the director is perpendicularly aligned with respect to the surface, the total charge must be *s*=+1 and the defect must be contained inside the spherical volume, thus no defects on the surface are allowed[40,43,44].

In droplets there are two known distinct point defects named hedgehogs and boojums, whose formation lies in the director field orientation in respect to the surface[45,46,47].

The first ones, hedgehogs, are formed in droplets with homeotropic anchoring conditions (perpendicular alignment of liquid crystal molecules around the surface). In this case

the director forms a radial-like configuration with a point defect in the center, which is in fact a 3D defect, they can exist in the bulk as well as on the surface – Figure 1.3 a).

In droplets with planar anchoring, the 2D point defects arise on the surface of the drop. These are essentially surface defects that cannot escape into the third dimension - move inside the nematic bulk - because of the boundary conditions. Due to this distinction, these surface defects are called boojums – Figure 1.3 b) [48] .

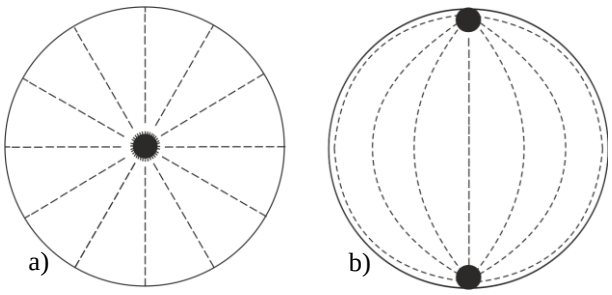

Figure 1.3 - Schematic of the nematic drops with different structures a) radial drop, with a hedgehog at the center of the sphere, regularly observed when the anchoring is perpendicular; b) bipolar drop, with two s=1 splay-type boojums located on the surface, which can be observed for planar anchoring conditions.

All this fascinating and complex behavior observed in the droplets and shells of liquid crystals, results from the ability of curved surfaces to contort the director field configuration, leading to complex director structures. However even more complicated defect configurations are expected when the liquid crystal is encapsulated inside regions with more complex topologies, such as tori, a topic that remains largely unexplored from the experimental point of view[42].

Geng *et al.* [4] have for the first time freely suspended a liquid crystal droplet in air, showing its properties to be extremely sensitive to changes in the surrounding environment. Another confinement is imposed by inserting a micro fiber through one axis of the droplet, resulting in a topology equivalent to a torus. This experiment enabled us to observe and characterize very interesting structures and phenomena. Recently Geng *et al.* [4,37] in preliminary research have shown liquid crystal droplets which were freely suspended in the air that according to its preliminary research showed intriguing mesoscopic structures and optical features, properties that suggest new or enhanced applications.

During this project we will only focus on situations governed by strong anchoring conditions, ie, the director field lies either perpendicularly (homeotropic) or parallel (planar) to all points on the droplet wall. As a consequence there will not be any direct competition between the director´s orientation on the surface and all other elastic forces within the droplet.

1.5. Fibers and process

Seeking new properties along with new designs that would in the near future enable the incorporation in 3D microlasers, highly sensitive sensors or give rise to new applications one will focus on examining liquid crystal droplets pierced by fibers. [4]

As already discussed, the soft matter approach employed is highly susceptible to external stimuli. This same remarkable susceptibility that enhances existing properties and gives rise to outstanding new ones, turns out to be a real challenge when it comes to assembling the proposed system.

It becomes crucial to ensure a strong anchoring between the droplets and the electro spun fibers produced and stretched in the air. Therefore, the following condition must be satisfied: R>>K/W, meaning that the fibers produced must be in the submicron range.

They not only have to satisfy the condition mentioned above, but in addition they should be defectless so that is possible to correctly understand and interpret the behavior of the pierced droplets. Based on the work presented by Geng *et al.* [4,37] it is clear that whenever a droplet is pierced by a cylindrical fiber that goes through the axis of the droplet, an additional surface is added along the droplet´s axis. Not only the droplet´s topology is changed, but new and more complex structures with unknown properties can be identified.

Despite the existence of several other methods for producing ultrathin nanofibers such as phase separation, template and self-assembly, electro spun fibers exhibit a wide range of unique features and properties such as high surface-volume ratio, since theoretically they can have indefinite length and can be spun from almost all materials on the basis of melts or solutions.

Even though this technique was discovered for over a century by Antonin Formhals[49], it was only in the nineties that it was fully established when Doshi and Renecker reintroduced as a simple way to make submicron fibers [50].

The electrospinning process is characterized by three major regions: cone region, steady jet region and the instability region.

In the first stage, a pump forces the fluid to come out of the syringe, forming a pendent drop at the nozzle, which is then electrically charged due to the high potential applied. Once charged, the droplet is deformed, acquiring a conical shape - known as Taylor cone - due to the competition between two forces: electrostatic and surface tension. At a certain critical electric field a fluid jet is ejected from the apex of the Taylor´s cone.

The behavior of the steady jet has been addressed theoretically to Taylor and Hohman *et al.* [51]. In this region, the jet travels along a straight path, where the diameter gets thinner as the jet moves away from the needle.

In the final region, the jet deviates from its coherent path and undergoes an instability called “whipping instability”. In order to understand and describe this behavior, Fridriech *et al.* [51]have presented a simple model suggesting that the jet reaches its terminal when the surface tension balances out the electrostatic charge repulsion. By this time, the jet undergoes a rapid movement and its outline is a spiral-like path.

The electrospinning set up is dependent upon numerous parameters, such as the distance from the nozzle to the target (change the electric field), the target shape, solution characteristics (solvent, concentration) as well as humidity and temperature.

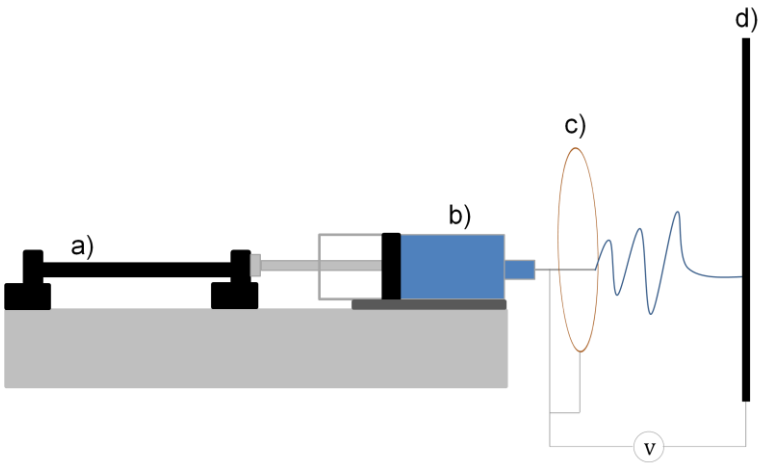

Figure 1.4 - Schematic representation of the electrospinning setup: a) peristaltic pump b) syringe c) coaxial shield ring d) target.

Chapter 2 – Experimental and Characterization Techniques

Liquid crystal droplets were obtained from the nematic liquid crystal 4´-n-pentyl-cyanobiphenyl (5CB) purchased from Merck, which exhibits a nematic phase in the temperature range from 18ºC to 34ºC.

The fibers were prepared from liquid crystalline hydroxypropylcellulose (HPC) and isotropic cellulose acetate (CA) solutions. HPC precursor solutions were prepared from 60% (w/w) hydroxypropylcellulose (HPC) (Aldrich, M_w=100000 $gmol^{-1}$) solutions in dimethylacetamide (DMac) purchased from Riedel-de Haen. CA isotropic solutions were obtained from 12% (w/w) cellulose acetate (Aldrich, M_w=61000$gmol^{-1}$, 40% acetyl groups) in a homogeneous mixture of 75% (w/w) acetone and 25% (w/w) DMac.

HPC as well as CA fibers were produced by electrospinning according with the procedure described previously by Yong et. al modified in the following way: the viscous solutions of HPC and CA were poured into a 1mL syringe (diameter 4.5mm) fitted with a 27-gauge needle (diameter 0.2mm) and 21-gauge needle (diameter 0.51mm) respectively. In both cases, the syringe was placed on the infusion syringe pump (KDS100) to control the polymer solution feed rate. A conducting ring, 15 cm in diameter, was held coaxially with the needle tip at its center, and electrically connected to it. Both the needle tip and the ring were directly connected to the positive output of a high voltage supply (Glassman EL 30 kV). After applying the electric potential between the metallic syringe-tip and the plate, the highly viscous polymeric solutions of HPC and CA were continuously fed to the syringe-tip at a constant flow rate of 0.04 mL h^{-1} and 0.2 mL h^{-1} respectively and accelerated by the ensuing electric field towards a collector consisting of two conductive stripes separated by a void gap of 0,5cm. The optimized operating conditions for the continuous drawing of cellulose derivative fibers were at a voltage of 15kV with a distance between the nozzle and the collector of 20cm for HPC, whereas for CA the optimized conditions were at a voltage of 10kV and a distance of 12cm. During the process the humidity was around 50% at room temperature, 23 ºC.

In order to obtain uniaxial aligned fiber arrays, fiber collectors made of two aluminum stripes (2.5x30mm) separated by a distance of 5mm were used. These specially designed frames allowed the HPC and AC fiber arrays to deposit across and consequently form suspended arrays. The fibers were then carefully dried under vacuum, at room temperature for 72 hours before further utilization. The fibers were characterized more thoroughly using a SEM DSM 962 model from Zeiss.

Two types of anchoring conditions were studied, it being known that the cellulosic fibers enforce tangential alignment for 5CB molecules [52], that the nematic liquid crystal aligns perpendicularly to the air interface and that a thin layer of glycerol ensures the planar anchoring of the confined liquid crystal at the surface.

In order to ensure the planar anchoring, nematic droplets were produced by mixing 5CB with glycerol in an optimized concentration, which was achieved by a thorough examination between cross and parallel polarizers.

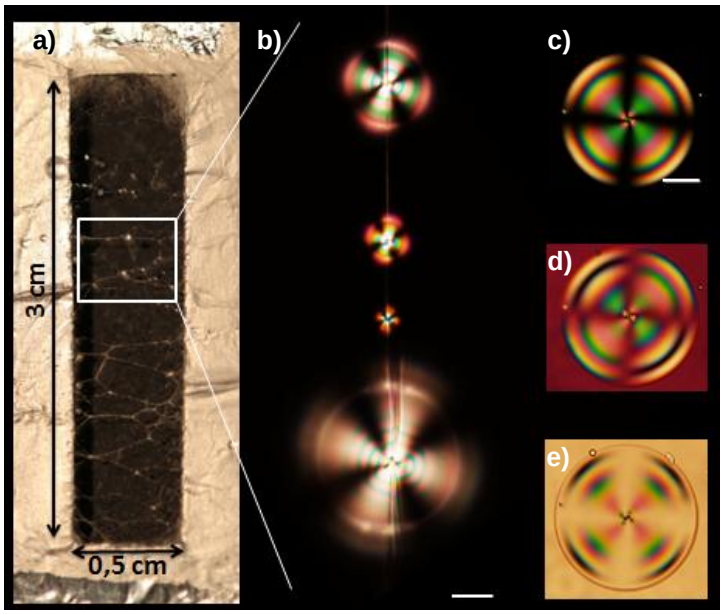

Figure 2.1 – Schematics of the experimental Setup. a) The electrospinning target used to produce the air suspended fibers with numerous 5CB liquid crystal droplets b) cross-polarized Figure corresponds to nematic droplets constrained on a 1,1 micrometers long fiber. c-e) Cross-polarized, with retardation plate and bright field Figures of 5CB droplets involved in optimized glycerol solution, planar anchoring.

The droplets were then carefully collected by means of a copper wire (0.1 mm) at room temperature and transferred to the suspended cellulosic electrospun fibers.

For further investigation POM pictures were taken using a transmission mode microscope, Olympus DP73 equipped with polarizers and a 530 nm retardation plate and a heating/cooling stage (Mettler, FP90).

POM analysis constitutes the main characterization tool so it deserves a brief explanation. As already mentioned in chapter 1.3 Nematic phase, the nematic liquid crystal used is uniaxially birefringent – as a result the incoming light when entering in the nematic liquid crystal material, breaks up in two different waves (extraordinary and ordinary) that travel at different velocities due to the existence of two different refraction index. For this reason whenever the nematic sample is placed between crossed polarizers, the incident light passing by the bulk material suffers a phase shift between the ordinary and extraordinary waves, meaning one assists to a change in the polarization state with respect to the incident light. In other words, a birrefringent material typically appears bright on a dark background. An exception arises when the local director field is aligned parallel to either the polarizer or analyzer so that no phase shift occurs.

Mapping the director field in these materials may be complemented by inserting a full wave retardation plate between the sample and the analyzer. The plate´s function is to retard the light propagation of a specific wavelength, 530nm.This way green light will be extinguished by crossed polarizers and the background field appears as magenta - complementary color.

However the light retardation of different wavelengths due to this full wave plate depends on the relative retardation of light, which depends, as already stated, of the nematic birefringence. Therefore if the retardation is not too severe, different nematic orientations appear either yellow, magenta or blue. If the nematic is aligned parallel or perpendicular to the polarizer, a magenta color is observed, whereas if the nematic is oriented along the direction of bottonm left to top right, a blue color is observed and if the nematic is oriented along a line from the top left to bottom right, a yellow color is observed. This simple description is valid only for nematic structures where the director doesn't rotate along the vertical direction[53].

Chapter 3 – Results and Discussion

3.1 Fiber characterization

Liquid crystalline droplets pierced by fibers, suspended in air, must satisfy the constraint R>>K/W for strong anchoring – defects regime - as explained in chapter 1.3.1.1. Hence a quantitative and qualitative analysis of the fibers is required prior to any droplet deposition.

The HPC fibers were prepared from solutions in the liquid crystalline phase (60% w/w), while CA fibers were obtained from isotropic solutions (12%). All fibers used were morphologically characterized by SEM.

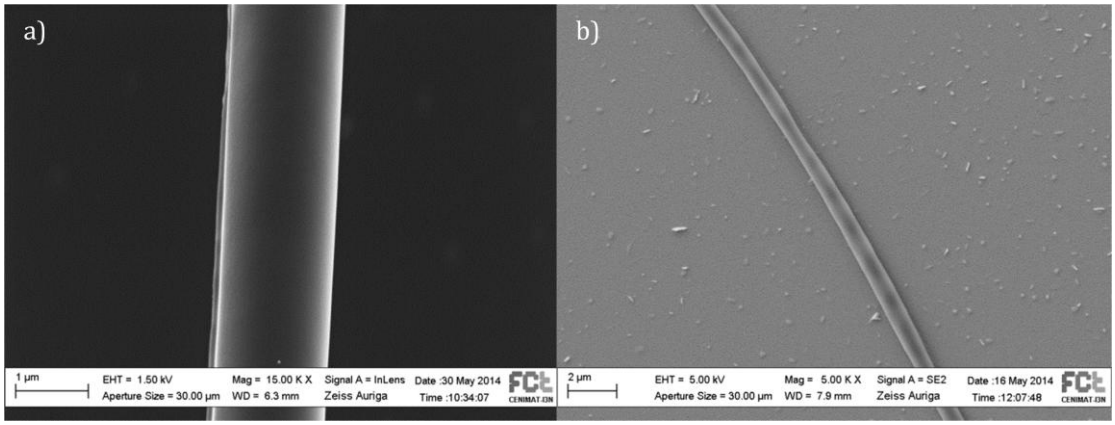

Figure 3.1 - SEM Figures of electrospun fibers a) cellulose acetate fibers produced from an isotropic solution (12%w/w) b) Surface modulated hydroxypropylcellulose fiber prepared from a solution in the liquid crystalline phase (60% w/w).

The SEM Figure 3.1 highlights the existence of a modulation on the HPC fiber surface. Moreover and as reported by Canejo *et al.* [54,55], HPC fibers produced from solutions in the liquid crystal phase adopt, on a supramolecular scale, a helically twisted form with the pitch measured in the micrometers range. This periodic structure on the HPC fibers is associated to the compound chirality, therefore right and left-handed fibers as well as perversion sites - that correspond to no handed sections - can be found, which may help explaining the modulation-effect on the fiber´s surface.

In contrast, the relatively low concentration of CA solutions ensures that the produced fibers are always in the isotropic phase, even when subjected to high shear rates (characteristic of the electrospinning process) so that no twist is presented nor is any surface modulation – uniform fiber.

The average diameter from CA fibers varies between 0,4 up to 1,2 µm, whereas thicker fibers are obtained from HPC, with their size ranging from 0,8 to 3 µm. These differences can be observed in Figure 3.1, as in Figure 3.3, however these were already expected, as the HPC solution in much more viscous than the CA solution. Nonetheless, all cellulosic-made fibers are defectless (due to process optimization) thus enforcing uniform boundary conditions for the nematic liquid crystal to align along the fiber axis.

These results show that the characteristic ratio, WR/K, is fulfilled, which is a crucial condition as it determines whether one is working (or not) in the topological defects regime.

3.2 Liquid crystal droplets pierced by cellulosic-made fibers

As previously reported cellulose-based fibers namely HPC and CA can induced a uniform planar alignment of 5CB molecules along the main axis of the fiber – schematically shown in figure 3.2 a) – giving rise to a hybrid shell - meaning the 5CB molecules are aligned in parallel to the fiber and perpendicularly to air interface[4,37,52].

For this particular set of conditions, molecules aligned in parallel with respect to the fiber main axis [52], show a gradual change as they are moving towards the surface, where molecules are locked perpendicularly to the surface (air interface) [24].

In a symmetrical droplet, this topological mismatch of the director field reaches its maximum in the center of the nematic liquid crystal leading to the formation of a hedgehog with topological charge +1, chapter 1.4.

Yet due to the pierced droplet not only the topology of the droplet is changed, as the breaking up of the droplet´s symmetry, by adding an additional cylindrical surface, generates the split of the hedgehog into a single disclination loop contained in a perpendicular plane with respect to the fiber with a +1/2 strength – so that Gauss theorem can be fulfilled[46,56].

By close observation of figure 3.2 b) it is possible to identify the characteristic disclinations ring defect: circular disclinations line in the middle of the droplet (in bulk) around the fiber which is placed symmetrically so that the lowest energy state is achieved.

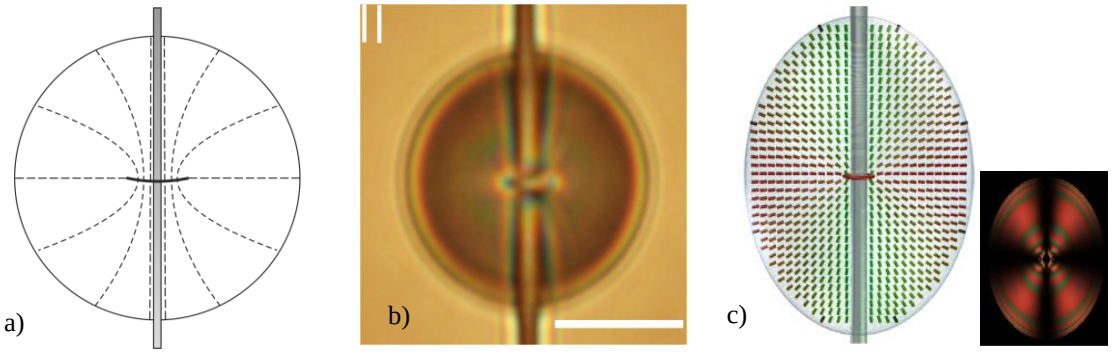

Figure 3.2 – Schematic of the director field configuration (a) air floating nematic shell constrained in a fiber, thus adding an additional cylindrical surface with planar anchoring along the droplets long axis and perpendicular at the outer surface (b) Bright field Figure example of a nematic drop threaded by cellulose acetate fiber. The Figure appears defocused to highlight the ring disclination. The scale bar corresponds to 10 μm (c) Numerically calculated structures in nematic drops threaded on cellulosic fibers with planar-homeotropic configuration. Courtesy of Prof. Zummer and his group.

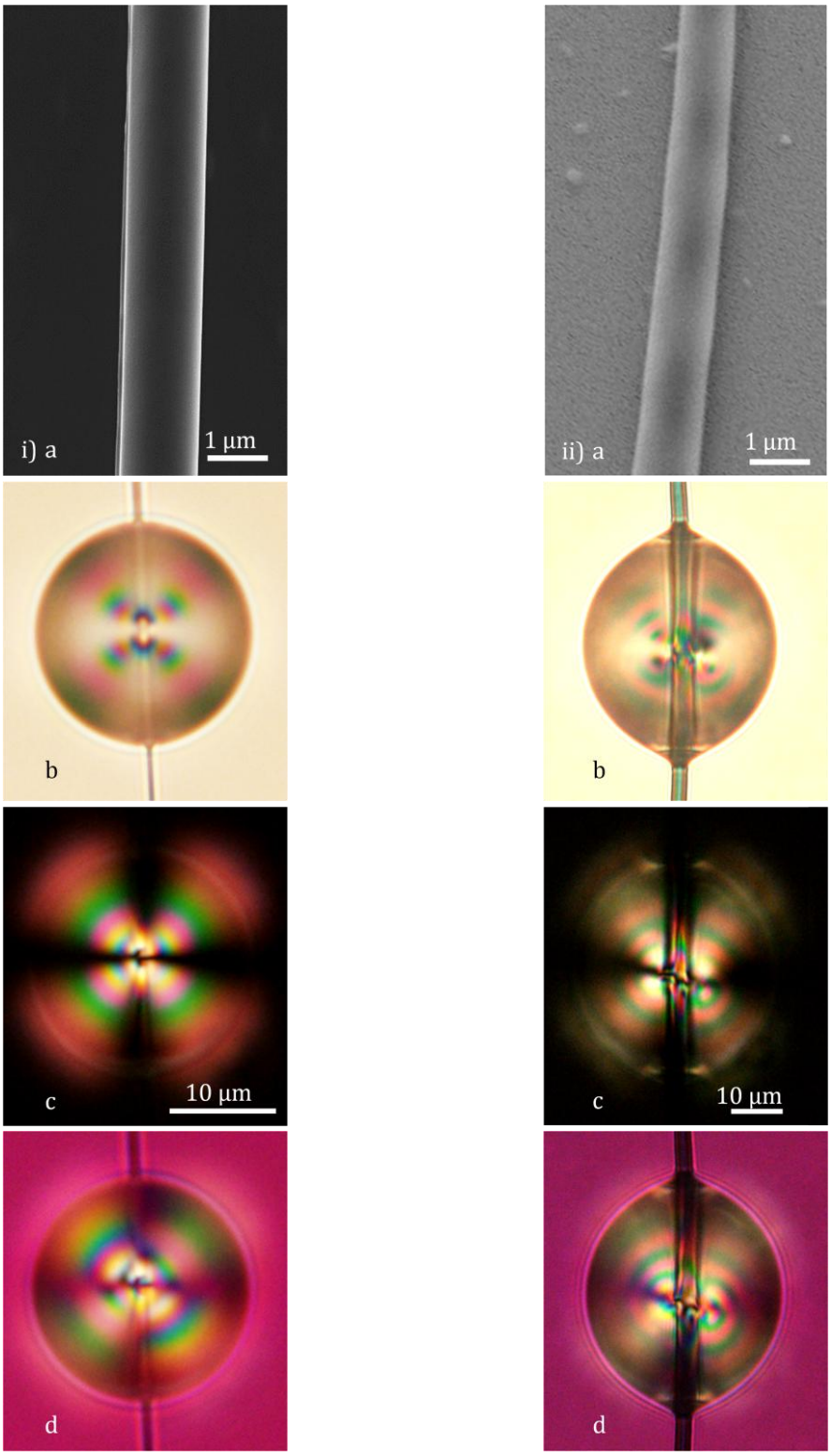

Figure 3.3 – SEM Figures of electrospun fibers and POM pictures of nematic bead textures. i) from cellulose acetate fibers produced from an isotropic solution (12%w/w) ii) hydroxypropylcellulose fiber prepared from a solution in the liquid crystalline phase (60% w/w). a) SEM Figures (b-d) POM pictures of 5 CB liquid crystal droplets threaded by a thin cellulosic-made fibers with planar anchoring at the fiber and homeotropic anchoring at the air interface b) under parallel polarizers c) under cross-polarizers picture d) with a 530nm full retardation plate, between cross-polarizers.

As already seen, whenever the director is tangentially anchored on the fiber surface and homeotropically at the air interface, a hybrid shell is formed that in turn causes a ring disclination I around the main axis of the fiber at the center of the droplet. Still, self-organized non-trivial structures of liquid crystals in specific geometries allows the detection of a weak external stimulus so that the response could be manifest as the structural change, directly observable using an optical microscope.

Here, micro-/nano-sized modulations on the fiber´s surface are amplified in the liquid crystal droplet. Periodic frustrations on the alignment conditions on the fiber, produce optically-detectable changes in the director field distribution at the macroscopic alignment as the liquid crystal molecules self-assembled with respect to these imperfections.

HPC fibers are known for their helical distortion as the lack of inversion symmetry produces chiral intermolecular forces that favor a twist of the principal axis of polymer chain alignment throughout the whole system[54,55]. In this way, a right- or left-handed bulk helicity is generated. This torsion-like effect onto the fiber´s surface forbids a continuous orientation profile of the director field inside droplet.

Conversely cellulosic-made fibers produced from the isotropic solution present no such feature, as there were never observed any ring inclination.

In figure 3.3 nematic droplets pierced by cellulose acetate showed no inclination of the ring. On the contrary, fibers threaded by HPC fibers showed a tilted ring, experimentally proving that the tilted rings observed on the HPC fibers are due to its inherently helical torsion that changes the surface´s boundary condition, which is proven by SEM characterization.

Additionally it is possible to visualize a shape difference in the droplets pierced by cellulose acetate and by hydroxypropylcellulose in figure 3.3: in the droplets pierced by cellulose acetate a spherical form is achieved whereas in the HPC case a rather ellipsoidal form is obtained. This behavior reinforces the existence of different surface properties of both cellulosic-based fibers acting upon the liquid crystal molecules.

In this way morphological periodic imperfections on the fiber´s surface on the molecular scale are highlighted in the droplet, as the nematic liquid crystal droplet exhibits leaned topological line defect in the bulk. Undoubtedly liquid crystal molecules gently follow the helical conformation of the fiber whereas in the absence of a fiber twist they lay planar to the fibers surface.

Of interest is the formation mechanism of the topological defect structure, namely the ring defect process. This study provides an important understanding of the formation and generation of the topological defects and the way in which they evolve towards the lowest energy configuration-field which remains largely unknown. In order to do so, the samples were heated above the nematic-to-isotropic transition temperature and subsequently cooled back at the same rate to room temperature.

The nematic-to-isotropic phase transition is characterized by an interplay between positional and orientational entropy, either promoting the rods to be randomly located or favoring them to be randomly oriented. Consequently as the temperature rises, the orientational entropy prevails, meaning interactions between molecules are rather weak, and that at a certain temperature – the transition temperature - molecules fully lose their alignment and become an isotropic fluid.

In this liquid-like state the droplet´s shape prevails on the fiber, however one could have expected that as this fully disorganized state is achieved, the droplet would have crumbled down and be consequently absorbed by the fiber – similarly to what happens when a water droplet is deposit in a cellulose acetate fiber.

This strongly indicates that the contact angle between liquid crystal droplet and the fiber is not simply ruled by the characteristic defects presented on the droplet, but by a more complex interaction.

The heating process represented in Figure 3.4 highlights the similarities of the nematic-to-isotropic transition in both cellulosic fibers with neutral rings, which one would have expected as in both examples the fiber is exclusively inducing the same planar degenerated anchoring effect on the 5CB molecules without any chirality-like effect, hence both cases will be explained as being essentially identical. For practical reasons, one will solely describe the phenomena in the droplet pierced by hydroxypropylcellulose.

The samples were heated from room temperature to about 0,1º C/min until the transition temperature. In the first 7 seconds the droplet preserves the overall shape and features, with no apparent changes, other than a gradual color change.

For t=7,5s, the ring defect – disclinations line - located at the center of the drop, starts to increase its diameter giving rise to the development of an isotropic droplet near the defect line. The appearance of an isotropic phase within the nematic phase below the critical temperature in the middle of the droplet is explained by understanding the consequences of a director field break down[57,58]. Discontinuities on the molecular orientation will have as a consequence an increase the local energy of the nematic phase, sufficient to depress the local nematic-to-isotropic transition temperature, meaning it is energetically more favorable for the transition to start near the ring rather than near the air interface, as one would have expected in the first place.

As a result of the formation of an inner isotropic drop within the nematic phase, a density difference between these two different regions is created, which results in a local thinning of the shell at one of the drop surfaces. Simultaneously the ring defect in the center vanishes due to the transformation of the boundary conditions, changing the nematic structure and the resultant defect configuration. By this time, the isotropic droplet tries to escape from the inner shell, t=8,7s. At the same time, a transition front sweeps the droplet inwards, discontinuously – for t=15,9. The color change observed throughout the increasing of the temperature may be explained by the decreased of the nematic layer thickness: the lower the nematic layer thickness, the more faded out the colors, t=24,5s.

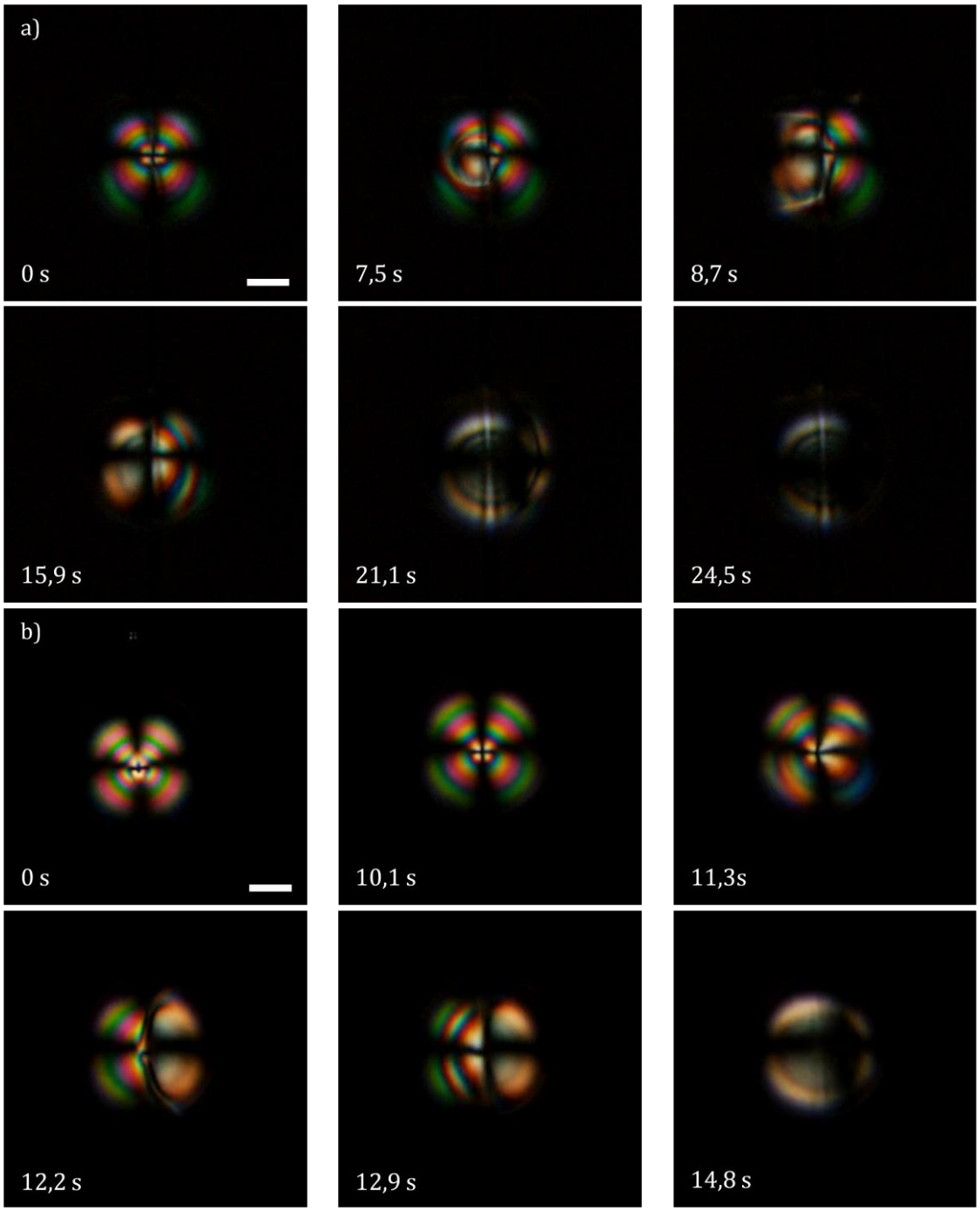

Figure 3.4 – Heating of a ring structure nematic droplet suspended in air. The heating rates are both equal to 1ºC/min. Heating snapshot Figures represent the time evolution of the nematic droplet from the equilibrium director configuration (t=0s) to the quasi-isotropic phase. a)droplet pieced by hydroxypropylcellulose fiber b) droplet pierced by cellulose acetate fiber. The scale bar corresponds to 10 µm.

Similarly to the heating process, no major differences were detected in the isotropic-to-nematic phase transition between the droplets pierced by HPC and CA fibers as was to be expected – Figure 3.5. This phase transition cannot take place unless the thermal fluctuations provide the nuclei of the more stable nematic phase enabling the system to overcome the energetic barrier.

Since orientations inside the droplet (isotropic phase) are equiprobable, the nematic phase growth process will start – randomly - near the outer surface of the droplet. As the system cools down, the molecular reorganization is enhanced, thus a thickening of the nematic layer is observed by the enhancement of the colors. Simultaneously to the nematic growth process, at t=20,5s the director bends towards one side of the droplet near the fiber surface - the fiber acquires a bigger role in the process as it constitutes a more favorable location, energetically speaking.[59]

By doing so, the director in the bulk does not distort appreciably, remaining very much tangentially oriented along the fiber main axis, giving rise to a transient disclinations line as showed for t=21,9s. The surface defect ring is subsequently formed at one of the sides in which the fiber crosses the nematic liquid crystal droplet, t=25,4s. Once no surface defects are allowed in this configuration - highly unstable – they migrate along the fiber main axis into the bulk, fixing at the center of the drop, t= 35,0s. The symmetrical location of this defect ring with respect to the original location results from the orientation of the nematic.

It is worth noticing the crosses seen for t=21,1s in Figure 9 and for t=0 in Figure 10, are solely projections of the polarizer´s configuration. These bizarre effects appear either in the beginning or in the end of the nematic to isotropic transition when there are already some nematic-like domains formed, thus reflecting somehow the molecular dynamics inside the droplet.

We have measured the initial velocity for the HPC fiber and CA fiber is approximately equal to v=112 μms^{-1} and 103μms^{-1} respectively. As the ring approaches the center of the droplet, one assist to a velocity decay, v=11 μms^{-1} and 9 μms^{-1} again for HPC and CA fibers.

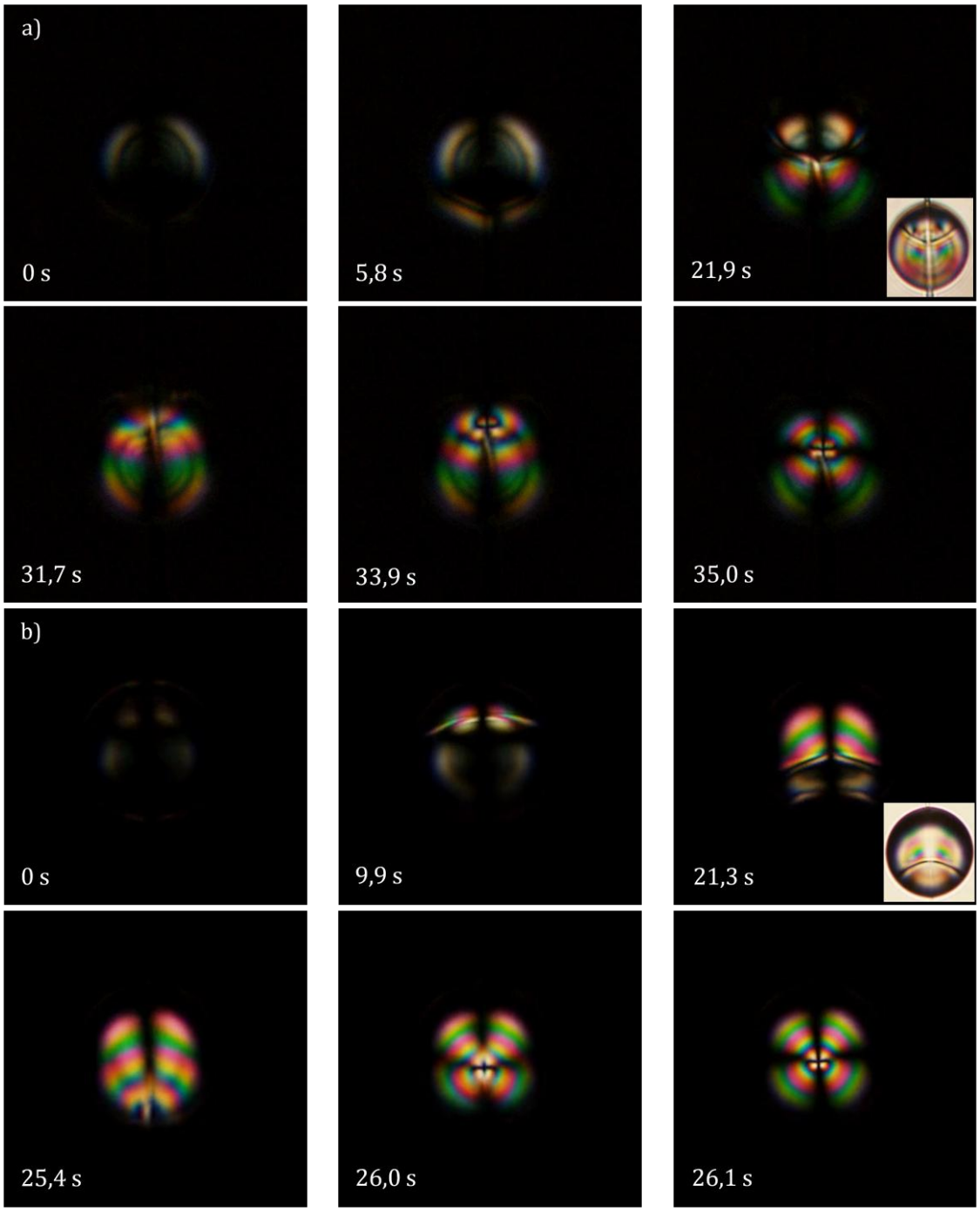

Figure 3.5 – Cooling processes of a ring structure nematic droplet suspended in air. The cooling rates are both equal to 1ºC/min. Cooling snapshot Figures represent the time evolution of the nematic droplet from the quasi-isotopic phase (t=0s) to the ring configuration. a) droplet pierced by hydroxypropylcellulose fiber b) droplet pierced by cellulose acetate fiber. The scale bar corresponds to 10 µm.

Figure 3.6 shows a droplet pierced by HPC and CA fibers covered by a thin layer of glycerol, so that a planar-planar configuration is ensured. This uniform distribution of the nematic director between the fiber and the nematic-glycerol interface is uniform, as a consequence the ring defect, typical of the planar-homeotropic configuration, is not present. This Figures corroborate the previous results presented in our research where the liquid crystal acts as an optical lens, as it amplifies the surface´s imperfections and defects by changing the director field and thus its topology namely the periodic twist found in the HPC fibers.

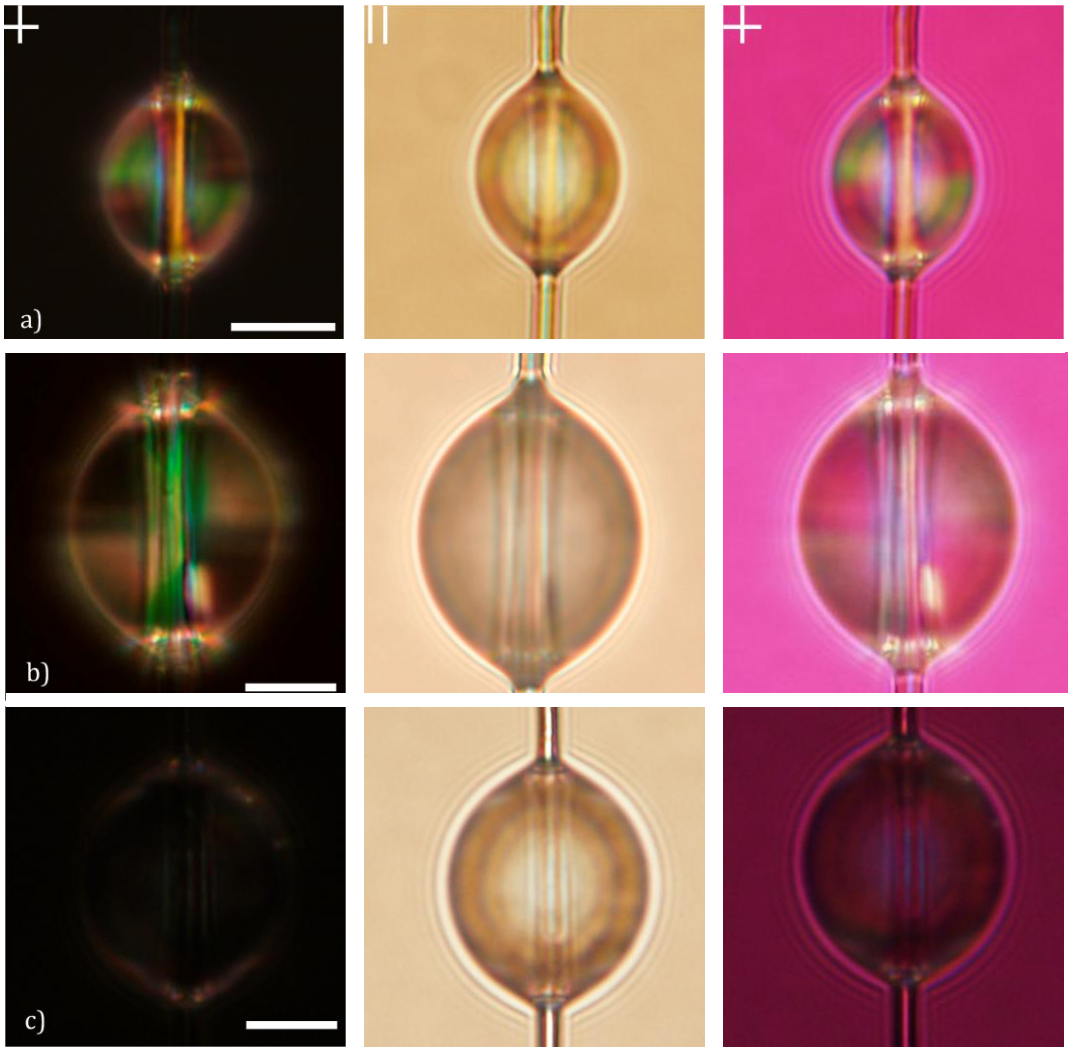

Figure 3.6 – POM Figures of 5CB droplets surrounded by a shell of glycerol which encloses the liquid crystal and suspended in air by a thin cellulosic-made fiber. (a-b) Hydroxypropylcellulose fiber prepared from liquid crystalline phase a) presenting a right-handed twist b) presenting a left-handed twist c) Cellulose acetate fiber prepared from the isotropic solution, presenting no-handed twist. The scale bar corresponds to 10 µm.

The internal (fibers surfaces) and external (glycerol or air) anchoring properties allow the study of liquid crystal droplets under different nematic director distributions, thus this thesis investigates not only the sensing properties of these type of materials, but also the influence of different exoteric configurations of the director field, by changing the anchoring conditions. At the same time, also the planar-planar configuration depends on the twist on the surface, as showed in the theoretical simulations Figure 3.7.

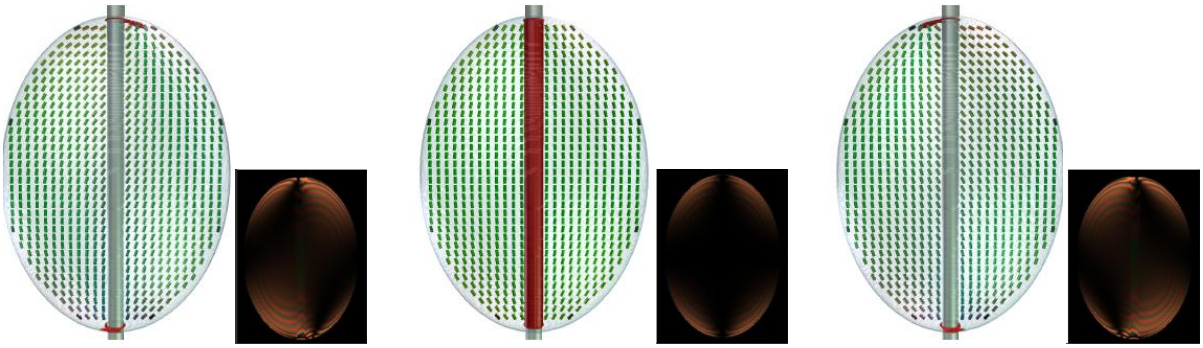

Figure 3.7 - Numerically calculated structures in nematic drops threaded on thin cellulosic fibers with planar – planar configuration a) right-handed fiber b) non-handed fiber c) left handed fiber. Note the resemblance of the micrographs with experiments, namely the ring location. Courtesy of Prof. Zummer and his group.

In this configuration, the droplet pierced by the CA fiber - prepared from the isotropic solution - Figure 3.6, has all its molecules perfectly aligned across the fiber main axis, therefore the droplet appears black under crossed polarizers as molecules are aligned parallel to the polarizer, so that there is no light shift.

Conversely, the periodic helical modulation onto the fiber´s surface forces the molecules to align themselves accordingly, leading to a new structure. The microscopic Figure under cross polarizers reveals dark sections in opposite quadrants of the droplet.

3.3 Liquid crystal droplets pierced by spider silk fibers

So far only cellulose-based fibers have been covered, however the acquired knowledge allows us to take this analysis further at exquisite designs that optimize function. Spider silks are known for their water-collecting capabilities as investigated by Zheng *et al*[60], where it was found that not only these fibers possess unique features enabling water-collection in microdroplets as their collection is directional[60].

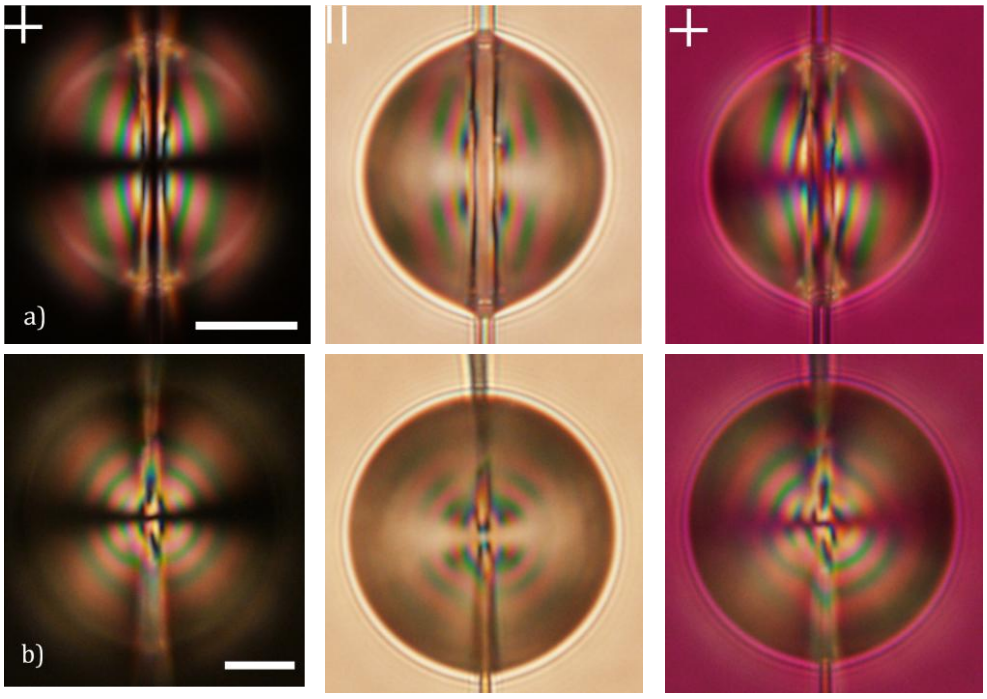

Figure 3.8 - POM pictures of nematic bead textures pierced by spider-made fibers. a) from an inner-spider b) from a garden spider. The scale bar corresponds to 10 µm.

Spider webs, besides fulfilling all requirements for strong-anchoring condition, have attracted much attention in recent years, specifically the understanding of their mechanical and aesthetic properties so that in a nearby future web-like materials can be artificially manufactured, replacing or enhancing existing materials or applications[61,62].

All spiders produce and use a wide variety of silks – each species can produce up to seven different high-performance silks - synthesized and spun by different glands – however only two types have been investigated. Although their amino acid composition is known, no consensus regarding the nano-organization has been reached. In addition the spider produces glue to coat the spiral silk accessory fibers.[3]

Figure 3.8 shows the 5CB nematic liquid crystal pierced in two different spider webs, which surprisingly showed at least two different configurations: figure 3.8 a), b). Moreover all configurations observed are completely different from the ones already seen when threaded by cellulosic-based fibers.

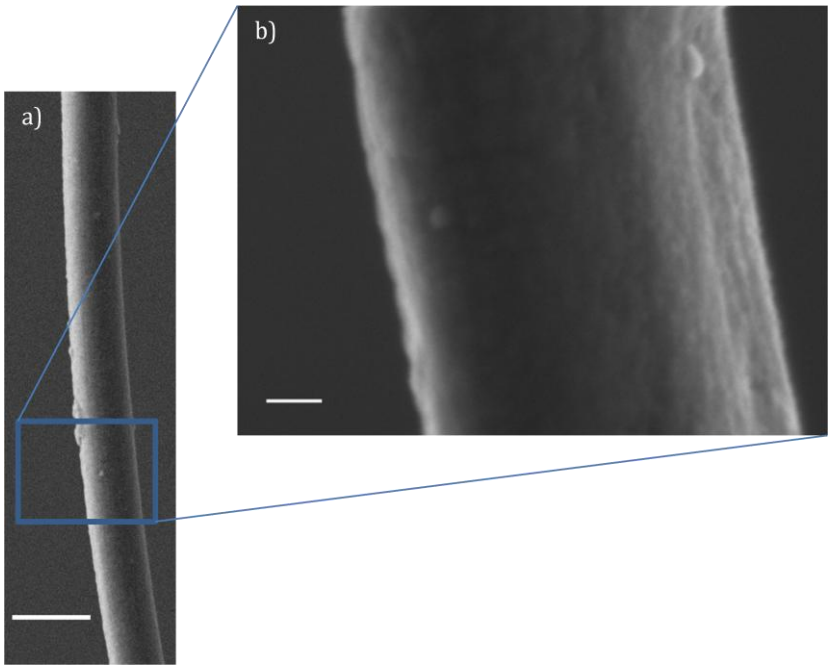

Figure 3.9 - SEM Figures of inner-spider web (droplet with no ring in the center) used to thread the 5CB liquid crystal with different magnifications in order to highlight the fiber´s surface.

The SEM Figure highlights the morphological differences between these and the cellulosic-made fibers, thus reinforcing the hypothesis that nano-sized discontinuities on the fiber surface are not only detectable, but amplified by the liquid crystal droplet, as their texture under polarized optical microscopy dramatically changes.

The absence of a ring disclinations in the center of the droplet showed in Figure 3.8 a) is the most obvious difference as it strongly indicates that the induced anchoring in the fiber has changed. Based on the theoretical simulation kindly provided by Zumer and his group and on SEM analysis of this particular fiber – figure 14 - we were able to infer that the inner-spider fiber, induces a infinite tangential anchoring on the liquid crystal molecules and therefore the ring disclination in the bulk of the droplet disappears, giving rise to two point defects apparently located on the surface – figure 3.8 a).

In the other case, figure 3.8 b), were the droplet is threaded by the garden spider, the appearance of a ring disclinations line is still unknown, as this particular spider fiber may enforce a planar configuration (similar to the one induced by the cellulosic fibers) or a slightly chiral tangential configuration instead.

In both cases further experiments and data analysis is required to undoubtedly determined the anchoring conditions on different spider silks.

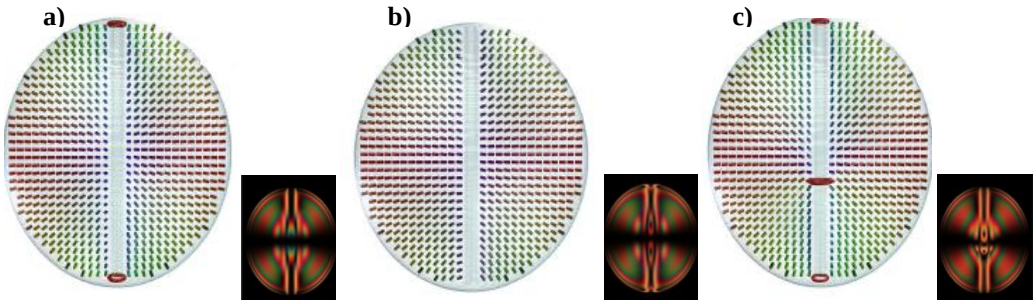

Figure 3.10 - Numerically calculated structures in nematic drops threaded on a spider web fiber suspended in air a) with infinite tangential orientation of the molecules at the fiber b) tangential at 45º c) with slight chirality. Courtesy of Prof. Zummer and his group.

Herein the importance of the role of the ring defect in the dynamic melting process is proven. Since there is no disclination ring, in contrast to all previous examples (HPC and CA) the droplet´s center is no longer a favorable place for the transition to start, but the droplets surface, as Figure 3.11 for t=27,1s might clarify this different behavior .

As temperature increases - Figure 3.11 a) - molecules on the fiber´s surface start losing their tangential alignment, accordingly there is a discontinuity in the director hence a transient defect ring is formed in the droplets center – t=28,5s. From here the dynamic behavior is qualitatively similar to the other found in the other fibers, as the main feature for any heating process is the formation of a disclinations line in the center of the droplet providing a stable and symmetrical site for the transition to occur.

The formation mechanism of the topological defect structure, figure 3.11 b), starts at the outer surface of the nematic droplet, as it is the first site to feel the temperature change.

The temperature decrease enhances the molecular re-orientation of the nematic in the bulk of the droplet, as one can see from Figure 3.12 for t = 10,7s. As the temperature further decreases, the fiber gains a preponderant role in the transition, similarly to the HPC and CA cases. Subsequently, a point defect is formed on the surface of the drop, for t=13,4s. However this energetically unstable state drives the systems to seek the lowest energy configuration, hence a closed line is formed and sweeps the droplet, t=18,2s, until reaching the opposite side where a second surface defect is formed. The system is now in equilibrium as both point defects are now located symmetrically and in opposite ends of the fiber.

As stated before, this droplet is characterized by having two surface rings in the end of the fiber´s main axis. The formation of the first ring occurs for t=10,7s. This energetically unfavorable condition forces the droplet to energetically compensate this, as the front phase transition sweeps the droplet from the side which the surface defect was firstly create to the opposite side: for t=13,4s to 27,1s. The phase transition ends when the two surface defects are symmetrically formed in each side of the droplet, thus ensuring the lowest energy state.

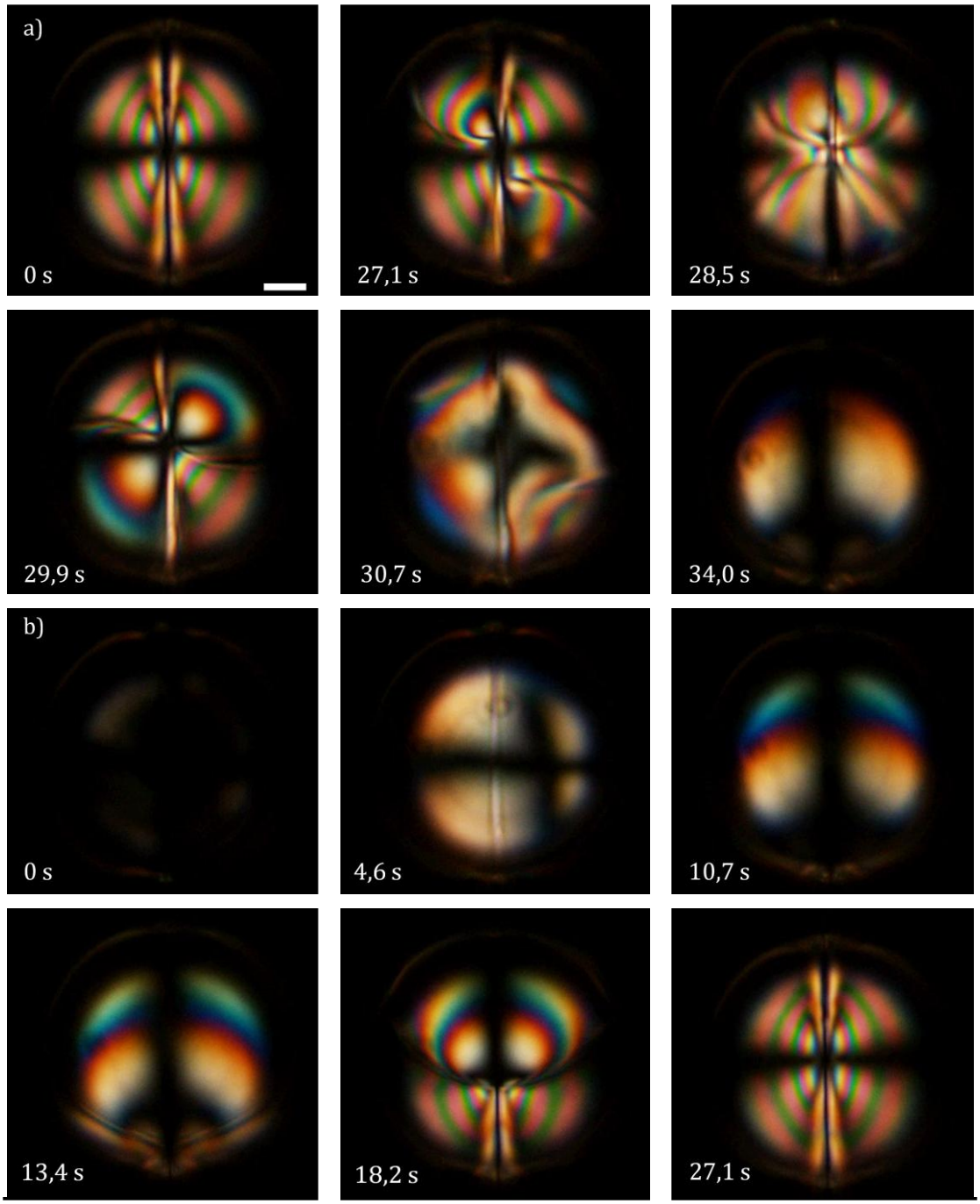

Figure 3.11 - Melting process of ring defects and ring defect generation process of a 5CB liquid crystal threaded by an inner spider web fiber with infinite tangential alignment at the fiber´s surface and suspended in air. a) Heating snapshot Figures represent the time evolution of the nematic droplet from the equilibrium director configuration (t=0s) to the quasi-isotropic phase (t=34s) at a constant heating rate of 0,1ºC/min. b) Cooling snapshot Figures represent the time evolution of the nematic droplet from the isotopic phase (t=0s) to the stable anisotropic configuration (t=93s) at a constant cooling rate of 1ºC/min.

The dynamic analysis of the droplet pierced by the garden spider, Figure 3.12, suggests a slight induced chirality by the fiber. However an increase in temperature consequently leads to an increase of the energy of the particles which reflects on the increase of the thermal fluctuations, allowing the liquid crystal molecules to move more freely.

At a certain point the thermal fluctuation outweighs the anchoring energy of the fiber, consequently the induced – chirality of the fiber plays a lesser role. At this point the molecules are rather tangentially aligned with respect to the fiber, than twisted.

The similarities between the picture 3.10 b) and the snapshot for t=58,8s support this hypothesis. A further increase in temperature leads to a total break up of orientational order from inside – out as already discussed in the other cases.

The formation mechanism of the topological defect structure is very similar to the one observed in Figure 3.11. Nonetheless the differences regarding the surface anchoring conditions promoted by the fiber, give rise to the formation of a point defect on the surface of the drop as the closed line shrinks and disappears. This defect, similarly to the phenomena described in the HPC and AC fiber, migrates towards the center with a initial velocity equals to $v=107\ \mu ms^{-1}$, which drastically decreases as approaching the droplet´s center to $v=17\mu ms^{-1}$.

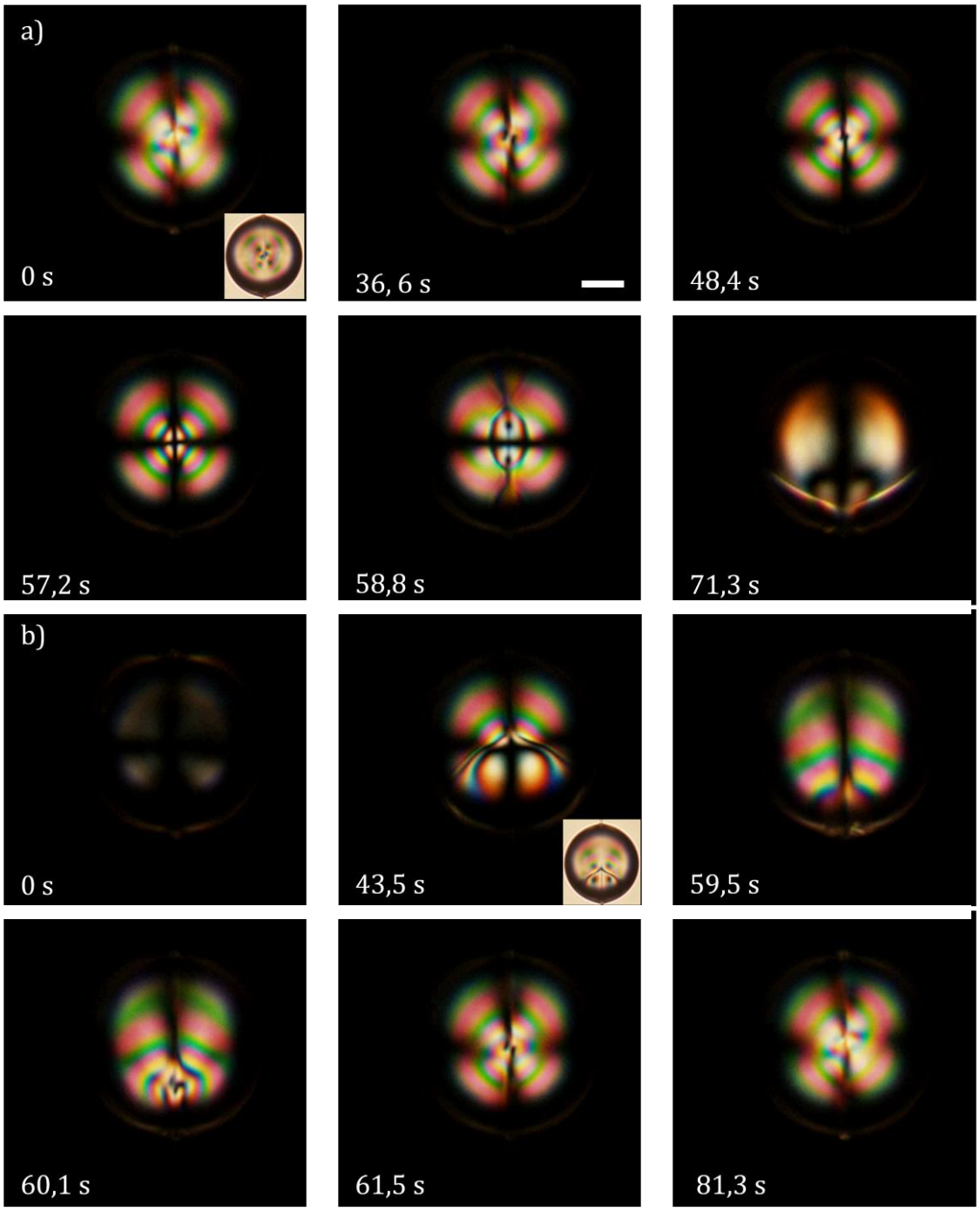

Figure 3.12 - Melting process of ring defects and ring defect generation process of a 5CB liquid crystal threaded by a garden spider web fiber with slightly chiral alignment at the fiber´s surface and suspended in air. a) Heating snapshot Figures represent the time evolution of the nematic droplet from the equilibrium director configuration (t=0s) to the quasi-isotropic phase (t=71,3s) at a constant heating rate of 0,1ºC/min. b) Cooling snapshot Figures represent the time evolution of the nematic droplet from the isotopic phase (t=0s) to the stable anisotropic configuration (t=81,3s) at a constant cooling rate of 1ºC/min.

Chapter 4 – Conclusions and Future Perspectives

Here, we report a simple method that tangibly visualizes surface conformations by using liquid crystal droplets. In this system, nematic liquid crystal droplets act as surface defect amplifying lenses taking advantage of the molecular behavior towards a conformation on the surface: molecules find themselves aligned with respect to the microgrooves or to any other smooth periodic imperfections that are located on the fiber´s surface. The nematic liquid crystal droplets threaded by different types of fibers, namely cellulose-based and more complex fibers, such as spider-web fibers, allowed to conclude that each fiber presented a typical morphological structure and thus different configurations of the director field distribution were possible to visualize. As mentioned, these evident changes on the droplet´s strucutre reflect the molecular alignment within the droplet, therefore SEM analysis enabled to detect specific differences of the different types of fiber.

In this work only uniaxial nematic liquid crystals were used, however, it would be of great interest to use different types of liquid crystals, such as biaxial nematic liquid crystals or nematic liquid crystal with a smectic transition.

In the first ones, quick identification between uniaxial and biaxial nematic is still a major problem. Likewise the existence of low-molar-mass thermotropic systems, although theoretically predicted, has not been experimentally confirmed, hence a 3D visualization system, as here reported, where a droplet is pierced by a nano-fiber, would be of great interest to confirm (or not) the existence of this phase.

In a less theoretical point of view, the smectic phase could be of grand significance concerning optical tuneability, as they could be used simultaneously with nematic phases for different purposes and ends.

Concerning the helical properties presented, in particularly, by the HPC fibers, it would be of point of view, proving that this ring inclination is solely caused by the left or right twist of the fiber constitutes a great challenge as the droplets are three dimensional mirrors of each other. This way the ring´s inclination is merely an indicator of the mechanical induced chirality of the fiber. Therefore the only way of knowing with certainty whether one is looking at a left or right-handed fiber is through the observation of the droplet with a retardation plate, allowing a qualitative analysis of the molecule´s orientation. Yet perfect conditions of observation regarding surface alignment, thickness and surface uniformity, ratio fiber/droplet would be of major importance/concern.

Even though it is not possible to unequivocally state that a certain fiber/section/region is either left or right-handed, it has been undoubtedly proven the effect of the induced mechanical great interest the possibility to distinguished right-handed from left-handed twists, however from the experimental chirality of the fibers on the molecular ornament.

Concerning the ring defect generation process and the melting of the ring defects – phase transition – one was able to conclude that the ring velocity solely depends on the liquid crystal´s elastic constant. Still more work would be of considerable interest in order to exactly understand the phenomena, as it could lead to great advances in fundamental physics and consequently for futuristic applications, regarding tuneability, self-assembly, sensing. However turbulent dynamic behavior on liquid crystals is extremely difficult either from the theoretical as from the experimental point of view, as it requires highly controlled environments.
In this context and regarding the role played by the topological defects, the work carried out suggests that the nematic-to-isotropic phase transition is in fact defect - driven, rather than some other mechanism driving the transition and the phenomena observed in the defects are solely a consequence. Still, further studies, namely with different configurations of the director field, would help supporting this hypothesis.

At the same time, studying the contact angle between liquid/liquid/solid interfaces as well as would be highly intriguing to investigate the dynamic contact angle between these different configurations and the role played by the defects, whose influence is known, yet not

quantitatively nor qualitatively. Investigations in this field would be of great interest for microhydrodynamics and consequently microfluidics.

Bibliography

[1] E. Feigenbaum and M. Orenstein, “Optical 3D cavity modes below the diffraction-limit using slow-wave surface-plasmon-polaritons.,” *Opt. Express*, vol. 15, no. 5, pp. 2607–12, Mar. 2007.

[2] V. S. R. Jampani, M. Humar, and I. Muševič, “Resonant transport of light from planar polymer waveguide into liquid-crystal microcavity.,” *Opt. Express*, vol. 21, no. 18, pp. 20506–16, Sep. 2013.

[3] L. P. Silva and E. L. Rech, “Unravelling the biodiversity of nanoscale signatures of spider silk fibres.,” *Nat. Commun.*, vol. 4, p. 3014, Jan. 2013.

[4] Y. Geng, D. Seč, P. L. Almeida, O. D. Lavrentovich, S. Žumer, and M. H. Godinho, “Liquid crystal necklaces: cholesteric drops threaded by thin cellulose fibres,” *Soft Matter*, vol. 9, no. 33, p. 7928, 2013.

[5] M. Humar and I. Musevic, “3D microlasers from self-assembled cholesteric liquid-crystal microdroplets.,” *Opt. Express*, vol. 18, no. 26, pp. 26995–7003, Dec. 2010.

[6] T. Ohzono, T. Yamamoto, and J. Fukuda, “A liquid crystalline chirality balance for vapours.,” *Nat. Commun.*, vol. 5, p. 3735, Jan. 2014.

[7] R. B. Wehrspohn, H.-S. Kitzerow, and K. Busch, *Nanophotonic Materials*. Weinheim, Germany: Wiley-VCH Verlag GmbH & Co. KGaA, 2008.

[8] O. Guzmán, N. L. Abbott, and J. J. de Pablo, “Quenched disorder in a liquid-crystal biosensor: adsorbed nanoparticles at confining walls.,” *J. Chem. Phys.*, vol. 122, no. 18, p. 184711, May 2005.

[9] X. Chen, B. D. Hamlington, and A. Q. Shen, “Isotropic-to-nematic phase transition in a liquid-crystal droplet.,” *Langmuir*, vol. 24, no. 2, pp. 541–6, Jan. 2008.

[10] T. Araki, M. Buscaglia, T. Bellini, and H. Tanaka, “Memory and topological frustration in nematic liquid crystals confined in porous materials.,” *Nat. Mater.*, vol. 10, no. 4, pp. 303–9, Apr. 2011.

[11] I. Muševič, “Integrated and topological liquid crystal photonics,” *Liq. Cryst.*, vol. 41, no. 3, pp. 418–429, Sep. 2013.

[12] G. H. Brown and J. J. Wolken, *Liquid Crystals and Biological Structures*, First Edit. Academic Press, 1979.

[13] J. de Gennes, P. G.; Prost, *The Physics of liquid crystals*, Second Edi. Oxford University Press.

[14] M. Humar and I. Muševič, “Surfactant sensing based on whispering-gallery-mode lasing in liquid-crystal microdroplets.,” *Opt. Express*, vol. 19, no. 21, pp. 19836–44, Oct. 2011.

[15] P. Pieranski, Pawel, Oswald, *Nematic and Cholesteric Liquid Crystals*. Taylor & Francis, 2005, p. 616.

[16] D.-K. Yang and S.-T. Wu, *Fundamentals of Liquid Crystal Devices*. Chichester, UK: John Wiley & Sons, Ltd, 2006.

[17] P. J. Collings and M. Hird, *Introduction to Liquid Crystals : Chemistry and Physics*, First Edit. Philadelphia: Taylor & Francis, 1997, p. 1997.

[18] E. M. T. M.Warner, *Liquid Crystal Elastomers*, First Edit. Oxford Science Publications, 2003, pp. 1–4,96–97,106–108.

[19] N. Schopohl and T. Sluckin, “Defect core structure in nematic liquid crystals.,” *Phys. Rev. Lett.*, vol. 59, no. 22, pp. 2582–2584, Nov. 1987.

[20] D. Demus, J. Goodby, H. Spiess, and V. Vill, *Handbook of Liquid Crystals*. Weinheim, Germany: Wiley-VCH Verlag GmbH, 1998.

[21] G. V Tkachenko, *New Developments in Liquid Crystals*, First Edit., no. November. Vukovar: In-Tech, 2009.

[22] O. D. Lavrentovich, T. Ishikawa, and E. M. Terentjev, “Role of the Divergence Elasticity,” *Mol. Cryst. Liq. Cryst. Sci. Technol. Sect. A. Mol. Cryst. Liq. Cryst.*, vol. 299, no. 1, pp. 301–306, Jun. 1997.

[23] T. C. Lubensky, D. Pettey, N. Currier, and H. Stark, “Topological Defects and Interactions in Nematic Emulsions,” Soft Condensed Matter, Jul. 1997.

[24] M. Kleman and O. D. Lavrentovich, “Topological point defects in nematic liquid crystals,” *Philos. Mag.*, vol. 86, no. 25–26, pp. 4117–4137, Sep. 2006.

[25] I. Chuang, B. Yurke, A. Pargellis, and N. Turok, “Coarsening dynamics in uniaxial nematic liquid crystals,” *Phys. Rev. E*, vol. 47, no. 5, pp. 3343–3356, May 1993.

[26] J. Fukuda, H. Stark, M. Yoneya, and H. Yokoyama, “Interaction between two spherical particles in a nematic liquid crystal,” *Phys. Rev. E*, vol. 69, no. 4, p. 041706, Apr. 2004.

[27] H. Search, C. Journals, A. Contact, M. Iopscience, and I. P. Address, “Surface effects and anchoring in liquid crystals,” vol. 391, 1991.
[28] M. Humar, M. Ravnik, S. Pajk, and I. Muševič, “Electrically tunable liquid crystal optical microresonators,” *Nat. Photonics*, vol. 3, no. 10, pp. 595–600, Sep. 2009.
[29] I. Rasing, Th; Musevic, *Surfaces and interfaces of Liquid Crystals*. Heidelberg: Springer, 2004, p. 296.
[30] D. Lavrentovich, “Phase transition altering the symmetry of topological point defects (hedgehogs) in a nematic liquid crystal,” *Zh. Eksp. Teor. Fiz 91*. pp. 1237–1244, 1987.
[31] M. Carrasco-Orozco, W. C. Tsoi, M. O’Neill, M. P. Aldred, P. Vlachos, and S. M. Kelly, “New Photovoltaic Concept: Liquid-Crystal Solar Cells Using a Nematic Gel Template,” *Adv. Mater.*, vol. 18, no. 13, pp. 1754–1758, Jul. 2006.
[32] J. Schmidtke and E. M. Terentjev, “Polydimethylsiloxane-enclosed liquid crystal lasers for lab-on-chip applications,” *Appl. Phys. Lett.*, vol. 96, no. 15, p. 151111, 2010.
[33] G. Cipparrone, A. Mazzulla, A. Pane, R. J. Hernandez, and R. Bartolino, “Chiral self-assembled solid microspheres: a novel multifunctional microphotonic device.,” *Adv. Mater.*, vol. 23, no. 48, pp. 5773–8, Dec. 2011.
[34] J. Noh, H.-L. Liang, I. Drevensek-Olenik, and J. P. F. Lagerwall, “Tuneable multicoloured patterns from photonic cross-communication between cholesteric liquid crystal droplets,” *J. Mater. Chem. C*, vol. 2, no. 5, p. 806, 2014.
[35] I. Musevic, M. Skarabot, U. Tkalec, M. Ravnik, and S. Zumer, “Two-dimensional nematic colloidal crystals self-assembled by topological defects.,” *Science (80-.).*, vol. 313, no. 5789, pp. 954–8, Aug. 2006.
[36] H. Coles and S. Morris, “Liquid-crystal lasers,” *Nat. Photonics*, vol. 4, no. 10, pp. 676–685, Sep. 2010.
[37] Y. Geng, P. L. Almeida, J. L. Figueirinhas, E. M. Terentjev, and M. H. Godinho, “Liquid crystal beads constrained on thin cellulosic fibers: electric field induced microrotors and N–I transition,” *Soft Matter*, vol. 8, no. 13, p. 3634, 2012.
[38] S. Z. G. P Crawford, *Liquid Crystals In Complex Geometries : Formed by Polymer And Porous Networks*. Bristol: Taylor & Francis, 1996.
[39] P. S. Drzaic, *Liquid Crystal Dispersions*, First Edit., vol. 1. Singapore: World Scientific Publishing Co., 1998.
[40] O. D. Lavrentovich, “Topological defects in dispersed liquid crystals, or words and worlds around liquid crystal drops,” *Liq. Cryst.*, vol. 24, pp. 117–125, 1998.
[41] I. Chuang, R. Durrer, N. Turok, and B. Yurke, “Cosmology in the laboratory: defect dynamics in liquid crystals.,” *Science (80-.).*, vol. 251, no. 4999, pp. 1336–42, Mar. 1991.
[42] E. Terentjev, “Liquid crystals: interplay of topologies.,” *Nat. Mater.*, vol. 12, no. 3, pp. 187–9, Mar. 2013.
[43] T. Lopez-Leon and a. Fernandez-Nieves, “Topological transformations in bipolar shells of nematic liquid crystals,” *Phys. Rev. E*, vol. 79, no. 2, p. 021707, Feb. 2009.
[44] a. Fernández-Nieves, V. Vitelli, a. Utada, D. Link, M. Márquez, D. Nelson, and D. Weitz, “Novel Defect Structures in Nematic Liquid Crystal Shells,” *Phys. Rev. Lett.*, vol. 99, no. 15, p. 157801, Oct. 2007.
[45] S. Z. Lavrentovich, Oleg D., P. Pasini, C. Zannoni, *Defects in Liquid Crystals: Computer Simulations, Theory and Experiments*. Dordrecht: Springer Netherlands, 2001.
[46] G. E. Volovik, “Topological dynamics of defects: boojums in nematic drops,” 2010.
[47] G. P. Alexander, B. G. Chen, E. A. Matsumoto, and R. D. Kamien, “Colloquium: Disclination loops, point defects, and all that in nematic liquid crystals,” *Rev. Mod. Phys.*, vol. 84, no. 2, pp. 497–514, Apr. 2012.
[48] T. Lopez-Leon and A. Fernandez-Nieves, “Drops and shells of liquid crystal,” *Colloid Polym. Sci.*, vol. 289, no. 4, pp. 345–359, Jan. 2011.
[49] A. Formhals, Patent: “Process and apparatus for preparing artificial threads,” 500,238, 1934.
[50] J. Doshi and D. H. Reneker, “Electrospinning process and applications of electrospun fibers,” *J. Electrostat.*, vol. 35, no. 2–3, pp. 151–160, Aug. 1995.
[51] Z. Ramakrishna, Seeram; Fujihara, Kazutoshi; Teo, Wee-Eong; LOim, Teij-Cheng; Ma, *An Introduction to Electrospinning and Nanofibers*. Singapore: World Scientific Publishing Co., 2005, p. 401.
[52] N. Mori, M. Morimoto, and K. Nakamura, “Hydroxypropylcellulose Films as Alignment Layers for Liquid Crystals,” *Macromolecules*, vol. 32, no. 5, pp. 1488–1492, Mar. 1999.

[53] D. B. Murphy, *Fundamental of light microscopy and electronic imaging*. Wiley-VCH Verlag GmbH.

[54] J. P. Canejo, J. P. Borges, M. H. Godinho, P. Brogueira, P. I. C. Teixeira, and E. M. Terentjev, “Helical Twisting of Electrospun Liquid Crystalline Cellulose Micro- and Nanofibers,” *Adv. Mater.*, vol. 20, no. 24, pp. 4821–4825, Dec. 2008.

[55] M. H. Godinho, J. P. Canejo, G. Feio, and E. M. Terentjev, “Self-winding of helices in plant tendrils and cellulose liquid crystal fibers,” *Soft Matter*, vol. 6, no. 23, p. 5965, 2010.

[56] W. Wang and T. Hashimoto, “Application of Topological Theorems to Studies of Coalescence and Ordering Processes in Nematic Droplets,” *J. Phys. Soc. Japan*, vol. 65, no. 12, pp. 3896–3900, Dec. 1996.

[57] S. Kralj, S. Žumer, and D. Allender, “Nematic-isotropic phase transition in a liquid-crystal droplet,” *Phys. Rev. A*, vol. 43, no. 6, pp. 2943–2952, Mar. 1991.

[58] N. Priezjev and R. Pelcovits, “Disclination loop behavior near the nematic-isotropic transition,” *Phys. Rev. E*, vol. 64, no. 3, p. 031710, Aug. 2001.

[59] Y. Lansac, F. Fried, and P. Maïssa, “Phase transition and defects in a thin nematic film,” *Phys. Rev. E*, vol. 52, no. 6, pp. 6227–6239, Dec. 1995.

[60] Y. Zheng, H. Bai, Z. Huang, X. Tian, F.-Q. Nie, Y. Zhao, J. Zhai, and L. Jiang, “Directional water collection on wetted spider silk,” *Nature*, vol. 463, no. 7281, pp. 640–3, Feb. 2010.

[61] Z. Qin and M. J. Buehler, “Spider silk: webs measure up.,” *Nat. Mater.*, vol. 12, no. 3, pp. 185–7, Mar. 2013.

[62] F. Vollrath and D. P. Knight, “Liquid crystalline spinning of spider silk.,” *Nature*, vol. 410, no. 6828, pp. 541–8, Mar. 2001.

Appendix

The numerical simulations presented during the thesis, made by Professor Zumer and his co-workers, were based on the following conditions.

A continuum mean field Landau-de Gennes free energy approach is employed to model the nematic liquid crystal ordering in the nematic droplets. The tensorial order parameter Q_{ij} is used to construct the total free energy F, which is able to fully characterize also the defect regions.

The following LdG free energy F is taken

$$F = \int_{LC} \left\{ \frac{A}{2} Q_{ij} Q_{ji} + \frac{B}{3} Q_{ij} Q_{jk} Q_{ki} + \frac{C}{4} (Q_{ij} Q_{ji})^2 \right\} dV + \int_{LC} \left\{ \frac{L}{2} \frac{\partial Q_{ij}}{\partial x_k} \frac{\partial Q_{ij}}{\partial x_k} + 2 q_0 L \varepsilon_{ikl} Q_{ij} \frac{\partial Q_{ij}}{\partial x_k} \right\} dV \int_{\Sigma} \left\{ \frac{W}{2} (\bar{Q}_{ij} - \bar{Q}_{ij}^{\perp})^2 \right\} d\Sigma$$

where LC denotes the integration over the bulk of the liquid crystal (LC) and Σ over the surface of the droplet. The first term accounts for the variation of the nematic degree of order, i.e. the possible formation of singular defects; A, B; and C are material parameters. The second term penalties elastic distortions from the twisted cholesteric state with a single uniform helical axis, characterized by the pitch p_0. *L* is the elastic constant and $q_0=2\pi/p_0$ is the inverse pitch. As a measure of relative size of the droplet with respect to the chiral pitch, it is useful to present the pitch in units of the droplet diameter as $p_0=4R/N$, where effectively, *N* corresponds to the number of π turns the director would make in a non-continued cholesteric along the distance equal to the droplet diameter *2R*. The final term accounts for the LC interaction with the planar degenerate surface, where *W* is the anchoring strength and

$$\bar{Q}_{ij} = Q_{ij} + \frac{1}{3} S \delta_{ij}$$
$$\bar{Q}_{ij}^{\perp} = P_{ik} \bar{Q}_{kl} P_{ij}$$
$$P_{ij} = \delta_{ij} - v_i v_j$$

where v is the surface normal, δ_{ij} is Kronecker delta, S nematic degree of order and P_{ij} is the projector to the surface as defined by Fournier and Galatola. We minimize the total free energy *F* numerically by using an explicit Euler relaxation finite difference scheme on a cubic mesh. The surface of the droplet is modeled as a spherical shell of mesh points with thickness equal to the mesh resolution. The following numerical values were used:

$$A = -0{,}172 \times 10^6 Jm^3$$
$$B = -2{,}12 \times 10^6 Jm^3$$
$$C = 1{,}73 \times 10^6 Jm^3$$
$$W = 1 \times 10^{-3} Jm^{-2}$$

and for polarization micrographs n_o = 1:5 and n_e = 1:7 are used as ordinary and extraordinary indices of refraction. Polarization micrographs of nematic droplets are calculated with the Jones 2x2 matrix formalism. This formalism incorporates the locally variable birefringence of the nematic refractive index -typically the leading contribution- but neglects reflections and refractions on the droplet surface.

More specifically, in this formalism, the light beam is propagated along a chosen direction and the total phase shift between ordinary and extraordinary polarisations is accumulated. We repeat the calculation for 10 different wavelengths in the approximate radiation spectra of the black body at 6000K (i.e. the white light approximation). The results for each wavelength are then summed with weights of the RGB color spectra to form color Figures that reproduce experimental observations. The polarization micrographs are calculated for the director

structure scaled by a factor of 3 to the size of typical experiments for a more quantitative comparison.

Defects regime:

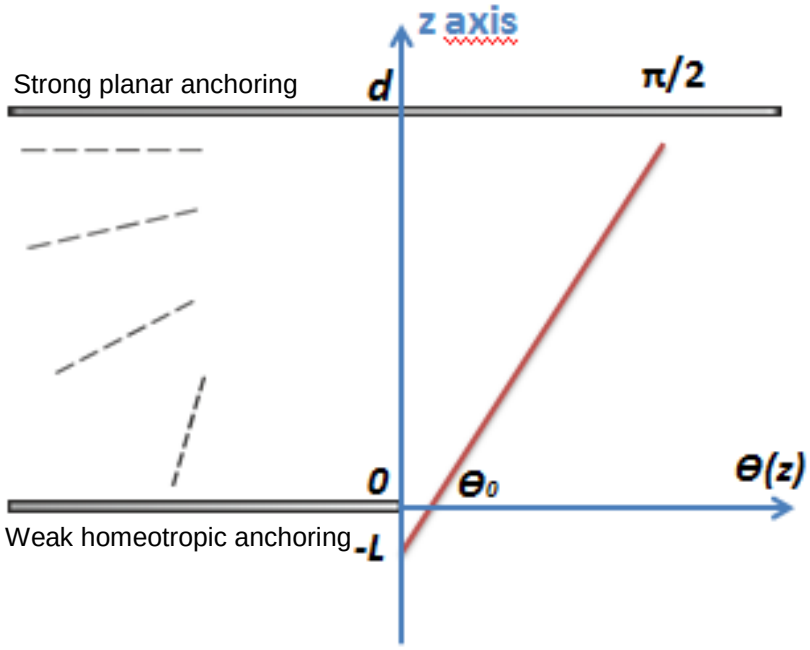

The equation (1.3) can be simplified by assuming that $K_{11}=K_{22}=K_{33}$. Then taking in account that the angle Θ_0 is the angle between the director and the normal to the fiber which can only vary with the z axis (distance in which the director passes from planar anchoring to weak homeotropic anchoring) and remains always in the same plane, the elastic constant k_{22} is negligible, as there is no twist contribution in this system.

Therefore, the equilibrium condition in bulk is given by:

$$K\frac{d^2\Theta}{dz^2} = 0$$

Once

$$\frac{d}{dz}\left(\frac{d\Theta}{dz}\right) = 0, \qquad \text{considering}\,\frac{d\Theta}{dz} = a$$

The expression of Θ that minimizes the bulk energy is given by:

$$\Theta = az + b$$

The constants that fulfill the equation above, can be found replacing by the following boarder conditions , which can be deduced from the schematic:

$$\Theta_0 = 0; z = 0$$

$$\Theta_0 = \frac{\pi}{2}; z = d$$

Therefore the solution an be written as following:

$$\Theta = \Theta_0 + \frac{\frac{\pi}{2} - \Theta_0}{d} z$$

The total energy of the system is a sum of the bulk energy and the anchoring energy. Yet, the anchoring energy is an energy per unit surface whereas the bulk energy is an energy per volume, therefore one should multiply the bulk contribution by d:

$$E_{total} = \frac{1}{2} K \left(\frac{\frac{\pi}{2} - \Theta_0}{d} \right)^2 d + \frac{1}{2} W {\Theta_0}^2$$

The above equation shows the energy variation for different angles of the director field. Therefore the minimum energy of the system is given by the following solution:

$$\Theta_0 \approx \frac{K}{W} \frac{\frac{\pi}{2}}{d} = \frac{L}{d} \frac{\pi}{2}$$

Where L=K/W which is the penetration length, see chapter 1.3.1.2.

Consequently, whenever $\Theta_0 \approx 0$, one is within the defects regime.

Equilibrium distance of the line disclination with respect to the fiber:

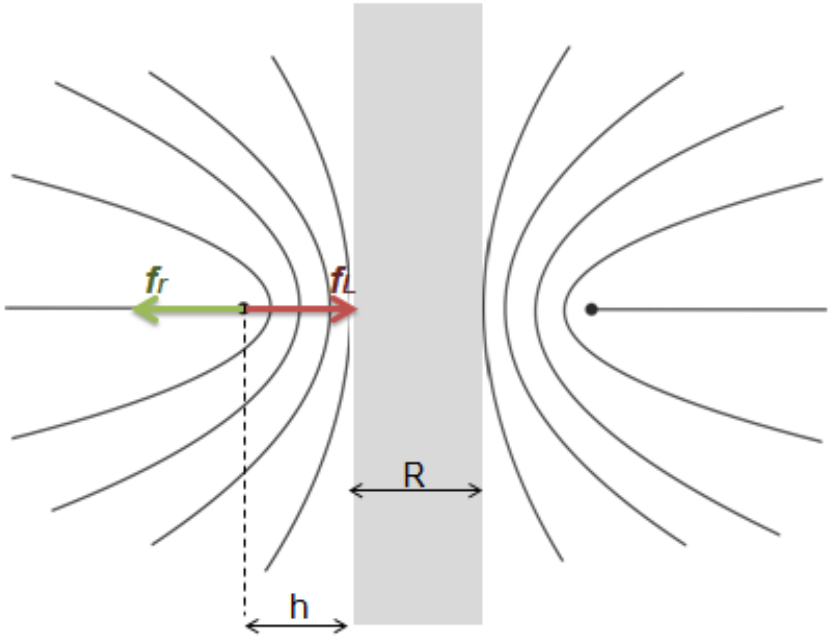

Upon the line disclinations defect, there are two forces acting:

$$f_r = 2\pi K \frac{m^2}{2h}$$

$$f_L = \frac{T}{R + h} \rightarrow f_L \approx \frac{T}{R}$$

Assuming that the e radius of the fiber is way larger than the equilibrium distance between the disclinations line and the fiber, h, one can approximate de Laplace force, f_L, as showed above.

As the ring disclination is in equilibrium and doesn't vanish throughout the medium:

$$f_r = f_L \rightarrow \frac{T}{R} = 2\pi K \frac{m^2}{2h}$$

Hence the equilibrium distance is given by, where *m* is the disclinations line strength (m=+1/2):

$$h = R\frac{\pi}{4}\frac{K}{T} \approx R\frac{K}{T}$$

Whereas the disclinations line tension, T, depends on the elastic constants and on the ratio between the radius of the droplet, R_d, and the radius of the defect core, r_c:

$$T \approx \pi K m^2 \left(ln\frac{R_d}{r_c} + \frac{1}{2}\right)$$